AUTOMATED OBSTRUCTIVE SLEEP APNEA (OSA) EVENTS CLASSIFICATION BY EFFECTIVE RADAR CROSS SECTION METHOD

A THESIS SUBMITTED TO THE GRADUATE DIVISION OF THE
UNIVERSITY OF HAWAII AT MANOA IN PARTIAL FULFILLMENT
OF THE REQUIREMENTS FOR THE DEGREE OF

MASTER OF SCIENCE

IN

ELECTRICAL ENGINEERING

DECEMBER 2020

By

Farjana Snigdha

Thesis Committee:
Olga Boric-Lubecke, Chairperson
Victor Lubecke
Yao Zheng

Keywords: Doppler Radar, Sleep Apnea Classification, Effective Radar Cross Section, Wireless Monitoring, Sedentary, Orientation, Cardiopulmonary

Dedicated to –

My Parents

Abul Hossain & Selina Hossain

Acknowledgement

First, I gratefully and sincerely thank my advisor Dr. Olga Boric-Lubecke for her continual guidance and invaluable supervision. Thank you for your countless advice and for your support in so many ways. Her continued support, experienced and immense knowledge helped me to finish my study. She not only acted as an advisor but also a guardian to me where I can always ask for advice and help regarding all aspects of my life besides study.

I would like to express my deepest appreciation to Dr. Victor Lubecke and Dr. Yao Zheng whose mentorship and encouragement enabled me to develop my research that lead to the findings in this dissertation.

I offer my sincere gratitude to my parents Abul Hossain and Selina Hossain who inspired me to go for the higher study and without whom this dissertation would not be possible. I am also grateful to my aunt Taslima Hossain to give me support and guidance in the most vulnerable times. I am also thankful towards my sisters, brother for being with me and encouraging me all the time.

Without any doubt, I am indebted to many of friends in Bangladesh and abroad who supported me. I also want to thank my friends of Hawaii whose friendship made this journey joyful and easy: Yousuf, Azmeary, Morsalin, Desiree, and Rafia. It is also a pleasure to thank my lab mates in the University of Hawaii for their assistance and friendship: Chancey, Mahmud, Khaldoon, Ehsan, Jordan, Ryan, Christine. During research they helped me with their knowledge and stayed beside me by their presence, support and encouragement.

Abstract

A sleep disorder is a medical disorder of the sleep patterns of a person which involves problem with quality, timing and amount of sleep. Obstructive Sleep Apnea (OSA) is one of the most common sleep disorders. OSA is briefly and repeatedly cessation of breathing when throat muscles intermittently relax and block the airway during sleep. Almost 22 million Americans suffer from sleep apnea, with 80 percent of the cases of moderate and severe obstructive sleep apnea undiagnosed. Often sleep disorder go undiagnosed as its diagnosis process is difficult and costly. Polysomnography (PSG) is considered as gold standard test for detecting sleep disorder. During PSG, different sensors are attached to suspected patient and performed in specific sleep clinic overnight in presence of a sleep technician. The patient must sleep in the clinic with different sensors attached to his body which is very uncomfortable. Multi-night PSG tests are rarely performed despite large night to night variance in sleep outcomes for those with OSA. Consequently, numerous alternative sleep monitoring technologies have been developed to overcome the disadvantages of full night PSG recording, using reduced number of sensors and allowing for at-home recording for natural sleep conditions of patient. In-home sleep monitoring system using Microwave Doppler radar is gaining attention as it is unobtrusive and non-contact form of measurement. Most of the reported results in literature focused on utilizing radar-reflected signal amplitude to recognize Obstructive sleep apnea (OSA) events which requires iterative analysis and cannot recommend about sleep positions also (supine, prone and side). In this dissertation, we propose a new, robust and automated ERCS-based (Effective Radar Cross section) method for classifying OSA events (normal, apnea and hypopnea) by integrating radar system in a clinical setup. In prior attempt, ERCS has been proven versatile method to recognize different sleep postures. Here, two different machine learning classifiers (K-nearest neighbor (KNN) and Support Vector machine (SVM) is employed to recognize OSA events from radar captured ERCS and breathing rate measurement from five different patients' clinical study. The proposed system has several potential applications in healthcare, continuous monitoring and security/surveillance applications.

Chapter 1 : Introduction

Chapter 2 : Literature Review

Chapter 3 : Doppler Radar System

Chapter 4 : Radar Cross Section

List of tables

List of Figures

List of Symbols

A Amplitude of the baseband signal (V)

A_{LO} Amplitude of the local oscillator signal (V)

A_{RF} Amplitude of the RF signal (V)

A_A Amplitude of signal returning from the abdomen (V)

A_T Amplitude of signal returning from the thorax (V)

u Ratio of A_A/A_T

Ar Ratio of arcs radii

a_H Amplitude of the heartbeat motion (m)

a_R Amplitude of the respiration motion (m)

a Radius (m)

α Phase offset (rad)

A_{eff} Effective area (m^2)

A_{ph} Physical area (m^2)

b Length (m)

β Propagation constant (rad/m)

d Largest dimension of the target (m)

d_S Diameter of the small sphere (m)

d_L Diameter of the large hemisphere (m)

D Largest dimension of the antenna (m)

Dr Ratio of displacement magnitudes

Δ Distance of maximum error on a spherical wave front (m)

E_i Incident electric field at the target (V/m)

E_r Reflected electric field at the receiver (V/m)

ε_n Integer coefficient in the RCS equation of a cylinder

f_o Local oscillator frequency (Hz)

ϕ_{in} Initial phase (rad)

ϕ_o Phase shift due to reflection from the surface of the body (rad)

ϕ_{tot} Total constant phase of the baseband signal (rad)

ϕ_{LO} Constant phase of the Lo signal (rad)

ϕ_{RF} Constant phase of the RF signal (rad)

$\phi_n(t)$ Generator phase nose (rad)

$\phi(t)$ Time varying phase modulation (rad)

G_T Transmitter antenna gain

G_R Receiver antenna gain

G Gain of identical transmitter and receiver antennas

G_1 Gain of the first LNA

G_2 Gain of the second LNA

G_{LNA} Total LNA gain

Γ_A Antenna power reflectance

Γ_{mix} Mixer power reflectance

j_n Spherical Bessel function of the first kind and order n

y_n Spherical Bessel function of the Second kind and order n

$_n h$ Spherical Hankel function of order n

i Imaginary unit

J_n Ordinary Bessel function of the first kind and order n

Y_n Ordinary Bessel function of the Second kind and order n

$_n H$ Ordinary Hankel function of order n

HR Average heart rate (bpm)

I_{LO} In-phase component at Lo input of the mixer (V)

Q_{LO} Quadrature component at Lo input of the mixer (V)

I_{BB} Baseband in-phase component (V)

Q_{BB} Baseband quadrature component (V)

IL_S Splitter insertion loss

IL_{fix} Fixed insertion loss

IL_{add} Additional insertion loss

IL_H Hybrid insertion loss

$IL_{5.8}$ Insertion loss specific for the 5.8 GHz system

k Variable in the motion delay offset

L Width of the effective area (m)

L_{conv} Mixer conversion loss

λ Wavelength (m)

n Variable in the roundtrip phase offset

$\Omega(t)$ Total time varying angle in the argument of I_{BB} and Q_{BB} (rad)

Ω_{max} Maximum total angle (rad)

Ω_{min} Minimum total angle (rad)

ω_o Angular local oscillator frequency (rad/sec)

P_s Scattered power (W)

P_T Transmitter power (W)

P_R Receiver power (W)

P_{in} Input oscillator power (W)

$P_{I/Q}$ RF power in the each of the quadrature receiver channels (W)

P_{LO} Power of the local oscillator signal (W)

p_n Scalar coefficient

q_n Scalar coefficient

R Radar target range (m)

$R(t)$ Instantaneous range of a moving target (m)

R_o Average range of moving target (m)

r Radial distance in spherical coordinates (m)

RF_{in} Voltage signal at the RF input of the mixer (V)

$\Re$ Gain factor of the link power budget of the Doppler radr (Ωm^2)

RR Average respiration rate (rpm)

S_i Incident power density (W/m^2)

S_r Received power density (W/m^2)

S_{LO} Voltage signal at the Lo input of the mixer (V)

S_{BB} Baseband signal (V)

σ Radar cross section (m^2)

σ_{eff} Effective radar cross section (m^2)

σ_{TM} Radar cross section for transverse magnetic field

σ_{TE} Radar cross section for transverse electric field

σ_{cal} Radar cross section of the calibration targets (m^2)

t Elapsed time (sec)

t_d Time delay (sec)

t_o Round trip time (sec)

θ Observation angle in spherical coordinates (rad)

V_{rms} Root mean square voltage (V)

v_T Velocity of the thorax during respiration (m/sec)

v_A Velocity of the abdomen during respiration (m/sec)

x Position on x-axis (m)

$x(t)$ Instantaneous torso displacement (m)

$x_H(t)$ Instantaneous heartbeat displacement (m)

$x_R(t)$ Instantaneous respiration displacement (m)

ψ Field solution for a point source (m^{-1})

Z Mixer RF input impedance (Ω)

Chapter –1

Introduction

Sleep is a dynamic process that varies from day to day, and hence it is important to measure multiple nights of sleep for medical, research, and wellness reasons. Home monitoring devices offer the potential to provide a more realistic platform in which many nights of sleep data can be captured. In remote health care, research in the design of affordable and reliable non-contact physiological monitoring systems is a very important goal for extending monitoring beyond the sleep clinic.

1.1 Research Problem and Scope:

Sleep apnea is highly prevalent in patients with cardiovascular disease. These disordered breathing events are associated with a profile of perturbations that include intermittent hypoxia, oxidative stress, sympathetic activation, and endothelial dysfunction, all of which are critical mediators of cardiovascular disease. Evidence supports a causal association of sleep apnea with the incidence and morbidity of hypertension, coronary heart disease, arrhythmia, heart failure, and stroke [1]. Cardiovascular disease (CVD) remains the leading cause of death in the United States, responsible for 840,768 deaths (635,260 cardiac) in 2016 [2]. Improving our understanding of sleep physiology and pathophysiology is an important goal for both medical and general wellness reasons. Almost 22 million Americans suffer from sleep apnea, with 80 percent of the cases of moderate and severe obstructive sleep apnea undiagnosed [1]. Polysomnography (PSG) is considered as gold standard for sleep apnea diagnosis which is carried out overnight in a specialized hospital-based sleep laboratory [3] with dedicated contact sensors and need a sleep technician. It is uncomfortable, expensive and the medical facilities have a small number of sleep technicians, leading to long waiting lists [4]. To guarantee natural conditions sleep monitoring, non-contact home monitoring technology is gaining increasing interest. Thus, a uniform, effective and automatic method is required which can determine sleep positions and sleep apnea events also to make the system robust.

1.2 Contribution:

In sleep studies and hospitals, a chest belt is often used to monitor a person's respiration, but these are obtrusive and can become uncomfortable to wear over time. Polysomnography (PSG) is the sleep study performed overnight while being continuously monitored by a credentialed technologist, is a comprehensive recording of the biophysiological changes that occur during sleep. The PSG monitors many body functions, including brain activity (EEG), eye movements (EOG), muscle activity or skeletal muscle activation (EMG), and heart rhythm (ECG), during sleep. It records at least 12 channels that require at least 22 sleep study wires that would be attached to the patient. All of this makes PSG time consuming, complicated, inconvenient, and expensive. For long-term continuous home-monitoring, doppler radar is gaining a lot of attention due to its non-contact and unobtrusive nature. Feasibility of utilizing Doppler radar system to identify different apnea events in reference to PSG system. However, that proposed system was not automatic as the system utilizes the amplitude-based technique to find different apnea events which requires extensive analysis [4]. In addition to that, ERCS has been utilized to recognize different sleep positions (supine, prone and side) [5]. It has been proved in various investigations that subject sleep positions play an important role in sleep quality and avoidance of certain sleeping position like supine may lead to decrease in the number and severity of obstructive episodes [6]. Thus, a uniform, effective and automatic method is required which can determine sleep positions and sleep apnea events also to make the system robust. In this dissertation, we investigated the feasibility of ERCS method for recognizing different OSA events (normal, apnea and hypopnea) from the clinical study with five different participants utilizing microwave Doppler radar system. In addition to that, we also integrated two different machine learning classifiers (KNN, SVM) to recognize different OSA events from ERCS and breathing rate measurement of the participants from` different episodes of the clinical study. SVM with quadratic kernel outperformed other classifier with an accuracy of 96.7%. The proposed system has several potential applications especially in in-home sleep monitoring system for adults and infants also (Sudden Infant Death Syndrome).

1.3 Thesis Organization:

Chapter 1 has presented an overview of the importance of automated sleep monitoring system which is comfortable and allows the multiple nights home-monitoring system at much lower cost. In this chapter, it also discussed about shortcomings of present gold standard sleep apnea detection system Polysomnography (PSG).

Definition of Obstructive sleep apnea (OSA), its classification (Apnea and hypopnea) and background about present sleep disorder monitoring methods are discussed in chapter 2. Chapter 2 also contains basic of Machine Learning and details of the classifier used in the thesis.

Chapter 3 explains the theory behind Doppler radar and its application in physiological monitoring. The radar architecture, demodulation algorithm, the system calibration and practical implementation are presented in this chapter.

Chapter 4 introduces the definition of radar cross section, its formulation, definition of Effective radar cross section (ERCS) and its measurement process.

Chapter 5 included the human testing data, details of PRMS system, classification of OSA events using machine learning, statistical analysis and measurement result.

Chapter 6 includes the human testing data, experimentation process, orientation recognition process for sedentary person using ERCS analysis.

The summary and conclusion are presented in chapter 7 where recommendation for future work are offered.

Chapter -2

Literature Review

Sleep is a naturally recurring state of mind and body, characterized by altered consciousness, relatively inhibited sensory activity, reduced muscle activity and inhibition of nearly all voluntary muscles and reduced interactions with surroundings. During sleep, the heart rate slows down, hormones and blood pressure fluctuates, muscles and other tissues relax, and metabolism slows down, allowing the body and mind time to rest and repair. People who cannot sleep well or at all are plagued with multiple difficulties such as a weaker immune system and lower cognitive function [7]. Sleep disorders are conditions that result in changes in the way that people sleep. A sleep disorder can affect overall health, safety and quality of life. Some of the signs and symptoms of sleep disorders include excessive daytime sleepiness, irregular breathing or increased movement during sleep. Sleeping disorders include dyssomnias, where sleep is difficult to enter or maintain, or in the case of hypersomnia is difficult to stay awake. They also include parasomnias, which relate to abnormal behaviors and actions that occur throughout the various sleep stages, and circadian rhythm sleep disorders, which affect the timing of the body's circadian clock [8]. Of all sleep disorders, one of the most widespread among the general population and serious is sleep apnea (SA). Obstructive sleep apnea (OSA) is one of the very common among various types of sleep apnea. Another forms of sleep apnea are central sleep apnea, and mixed apnea. Central sleep apnea is in which the brain fails to properly control breathing during sleep. Mixed apnea ids combination of obstructive sleep apnea and central sleep apnea. Obstructive sleep apnea is far more common than other sleep apneas. This chapter will define OSA, kinds of OSA along with present method in the literature for sleep disorder monitoring.

2.1 Non-invasive Physiological Monitoring:

Radar based physiological monitoring has been demonstrated in many studies for the feasibility of vital sign detection and physiological monitoring. Its wireless sensing capability eliminates electrodes attachment and offers comparable readings on a number of physiological parameters. Microwave doppler radar has been used to sense physiological movement since early 1970 [9]. In 1975 James Lin measured respiration signal of rabbit and human from a 30 cm distance using X-band sweep oscillator equipped with a rectangular horn antenna. He and his

team continued research on using the microwave for detecting apnea noninvasively and was published in 1977. Researchers also wanted to find both the respiration and heart rate. With the advancement of analog and digital signal processing, Chan and Lin could obtain heart and respiration signals separately in 1987. In 2002 Lubecke invented methods to make add-on module that uses signals from existing wireless devices to measure heart and respiration rates. Quadrature Doppler radars were developed, and different modulation techniques were proposed for accurate respiration and heart signal measurement. Techniques were also developed in last decades to compensate for distortion such as AC coupling distortion, I/Q channel imbalances, random body motion cancellation. Hybrid FMCW-interferometer radar was proposed for precise 2-D positioning and life activities surveillance. The proposed hybrid radar works in the 5.8 GHz ISM band with a 160 MHz bandwidth [10]. Without any electrodes attached to human body, reference comparable readings including respiration rate and heart rate [11] [12], heart rate variability [13], arterial pulse wave [14], and tidal volumes [15] can be extracted. Clinical studies were also conducted extensively to enhance the credibility of using Doppler radar as medical vital sign monitor. Cardiopulmonary activity and motion detection capabilities of the microwave Doppler radar offer paths for a number of practical applications, which were realized with complex algorithms for fall detection, occupancy sensing, in vivo tumor tracking, sudden infant death syndrome monitoring, and obstructive sleep apnea study. Due to its penetration ability, microwave signal not only can go through objects such as clothing for vital sign detection, it is also able to penetrate concrete walls or obstacles for through-the-wall sensing and rescue operations.

Doppler radar life sign sensing relies on the detection of chest wall motions associated with cardiopulmonary activities. When operating, microwave signal transmitted by medical Doppler radar system working at ISM (Industrial, Scientific and Medical Radio) band with Federal Communications Commission (FCC) allowed radiation power is shined on human subjects' chest area for detecting small displacement triggered by heartbeat or respiration. By gathering the Doppler shift content in backscattered signal from the air-skin interface, the variations of the chest wall location as regard to radar can be discerned. It provides safe, clean, non-invasive and non-contact medical-grade measurement for heart rate and respiratory rate readings.

2.2 Obstructive Sleep Apnea (OSA):

There are several types of sleep apnea, but the most common is obstructive sleep apnea. Obstructive sleep apnea (OSA) is a potentially serious sleep disorder. It is a sleep-related breathing disorder that involves a decrease or complete halt in airflow despite an ongoing effort to breathe. It occurs when the muscles relax during sleep, causing soft tissue in the back of the

throat to collapse and block the upper airway [AASM pdf]. A noticeable sign of obstructive sleep apnea is snoring. It causes breathing to repeatedly stop and start during sleep. OSA that is associated with excessive daytime sleepiness is commonly called obstructive sleep apnea syndrome. These obstructive events usually result in measurable drops in blood oxygen saturation, which returns to baseline levels when the person's breathing resumes. Episodes of OSA typically end with the person waking up briefly to reopen his or her airway.

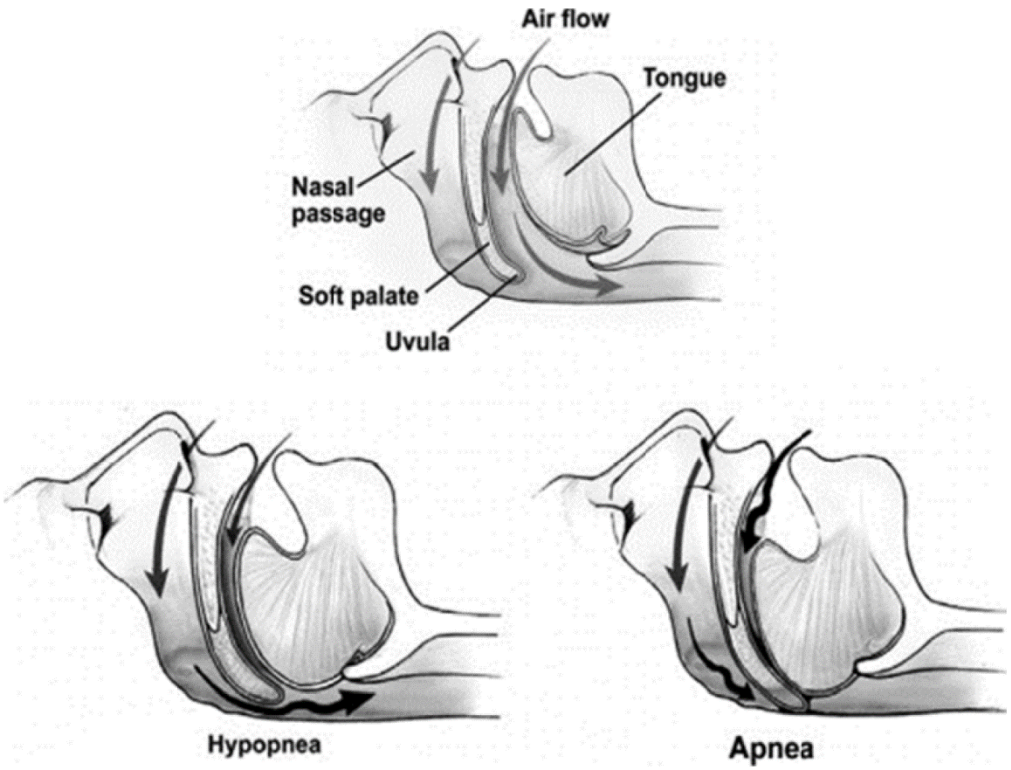

Fig 2.1: Partial and complete airway obstruction during hypopnea and apnea. Reprinted from Hahn PY, Somers VK. Sleep apnea & hypertension. In Lip: GHY, Hall JE, eds. Comprehensive hypertension. St. Louis, MO:Mosby; 2017:201-207. Copyright Elsevier

Obstructive sleep apnea is basically two types. One is Hypopnea and other is Apnea. Hypopnea is overly shallow breathing or an abnormally low respiratory rate. Hypopnea is typically defined by a decreased amount of air movement into the lungs and can cause oxygen levels in the blood to drop. It commonly is due to partial obstruction of the upper airway. As defined in American Academy of Sleep Medicine (AASM), hypopnea presents a 70% or more reduction compared to normal baseline accompanied by more than 3% oxygen desaturation or arousal [AASM pdf]. Apnea is the cessation of breathing. During apnea, there is no movement of the muscles of inhalation, and the volume of the lungs initially remains unchanged. Voluntarily doing this is called holding one's breath. As defined in American Academy of Sleep Medicine (AASM), apnea presents a 90% or more reduction in airflow compared to the normal baseline.

2.3 Sleep Apnea Detection Techniques:

An evaluation of sleep apnea often involves overnight monitoring at a sleep center of breathing and other body functions during sleep. The gold standard for detecting sleep apnea is polysomnography (PSG). For Obstructive Sleep Apnea (OSA), a final diagnosis is usually obtained by a medical examination using a Polysomnography (PSG) test which is records the biophysiological changes that happen during sleep at a sleep lab. PSG test requires overnight screening with dedicated contact sensors and a sleep technician need to coordinate all these sensors. It is uncomfortable as many wires and sensors connected to patient, expensive and the medical facilities have a small number of sleep technicians, leading to long waiting lists. Due to unavailability of much comfortable, affordable detection system, many of sleep apnea patients goes undetected. Undiagnosed sleep apnea is directly tied to an increased risk in cardiovascular and metabolic health. Sleep apnea occurs in about 3 percent of normal weight individuals but affects over 20 percent of obese people, Jun says[4]. In general, sleep apnea affects men more than women. However, sleep apnea rates increase sharply in women after menopause. There is much need to improve the efficiency, diagnosis time, and accuracy of the PSG. New techniques are currently being developed and tested by bioengineers to improve upon the weaknesses of the PSG and help diagnose more patients more quickly.

2.3.1. Polysomnography:

The gold standard for Sleep Apnea detection is polysomnography (PSG). Polysomnography makes comprehensive recordings of the biophysiological changes that happen during sleep. The PSG monitors many body functions during sleep such as: brain activity (EEG), eye movements (EOG), muscle activity (EMG), heart rhythm (ECG), respiratory airflow and respiratory effort. PSG will typically record a minimum of 12 channels requiring a minimum of 22 wire attachments to the patient [16]. These channels vary in every lab and may be adapted to meet the doctor's requests. There is a minimum of three channels for the EEG, one or two measure airflow, one or two are for chin muscle tone, one or more for leg movements, two for eye movements (EOG), one or two for heart rate and rhythm, one for oxygen saturation, and one each for the belts, which measure chest wall movement and upper abdominal wall movement [16]. The movement of the belts is typically measured with piezoelectric sensors or respiratory inductance plethysmography. This movement is equated to effort and produces a low-frequency sinusoidal waveform as the patient inhales and exhales. Because movement is equated to effort, this system of measurement can produce false positives, especially during obstructive apneas, for effort to be made without measurable movement.

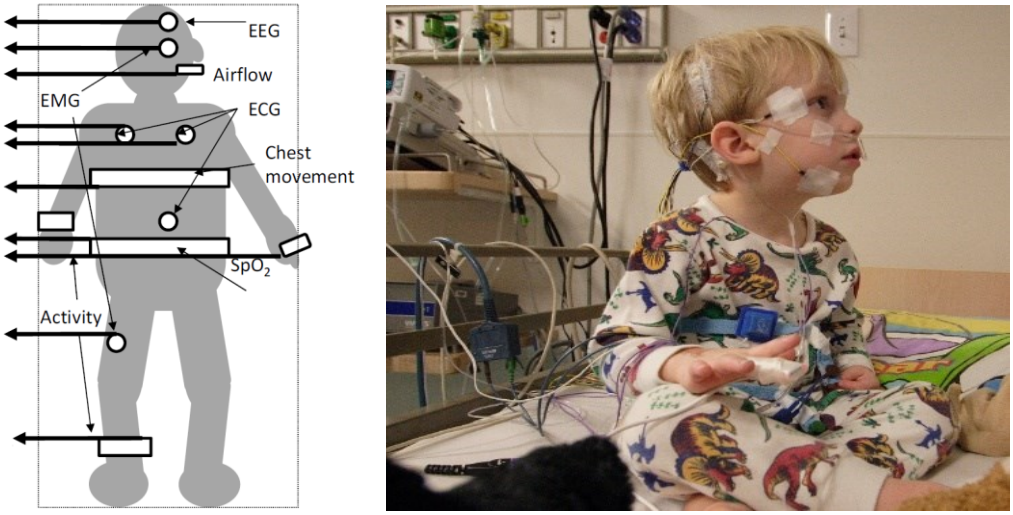

(a) (b)

Fig 2.2: (a) Diagram showing placement of different sensor for PSG test on a person's body
(b) Pediatric PSG patient with all sensors

After the test is completed a scorer analyzes the data by reviewing the study. The score consists of the following information: sleep onset latency, sleep efficiency, sleep stages and analyzing whole lot of data from all the sensors which is time consuming and difficult.

2.3.2 Other Contact Detection Techniques:

There are many contact devices introduced to detect Sleep apnea while some are reduced version of PSG means a smaller number of sensors are used to make it comfortable for patient. Also, less number of sensor compared to traditionally used in PSG make the detection of sleep apnea analysis part more easy and time duration is less than earlier for analysis.

Many studies show that OSA can be detected by the use of an Electrocardiogram (ECG), which measures cyclic variations in the length of heartbeats. During SA, the bradycardia (slow heart rate) normal during sleep is always followed by tachycardia (abnormally fast heart rate) upon its cessation [17]. Chazal et al. [18] presented an automated classification algorithm to determine sleep disorder period using the short-duration epochs of surface electrocardiogram data which were recorded during a polysomnography studies [18]. Later they proposed an automatic method of detecting sleep disorder including obstructive, mixed and central apneas, and obstructive, mixed and central hypopneas by analyzing the heart variability, an ECG based respiration signal and blood oxygen level with a pattern recognition system [19]. In another work,

Yilmaz et al. [20] proposed a method to detect paradoxical breathing epochs by extracting some features from only a single-lead electrocardiography (ECG) signal.

Many studies have shown that an Electroencephalogram (EEG) - a monitor of brain wave activity – can diagnose SA [21]. Electroencephalographic (EEG) arousal happens in EEG recordings when patient awakes from sleep. Sleep apnea events usually cause an arousal as a result of stoppage in respiration. Hence, the respiratory-related arousals is visible EEG recording. Hence, in [22] Sugi et al. presented a method to automatically detect EEG arousals in the EEG data recorded during PSG test.

Yadollahi et al [23] in his paper reported on developing a new system for OSA detection and monitoring, which only requires two data channels: tracheal breathing sounds and the blood oxygen saturation level. They developed a fully automated method that uses the energy of breathing sounds signals to segment the signals into sound and silent segments. Then, the sound segments are classified into breath, snore (if exists) and noise segments. The saturation level signal is analyzed to find the rises and drops in the signal. Finally, a fuzzy algorithm was developed to use this information and detect apnea and hypopnea events.

Snoring is always almost happening with obstructive sleep apnea as OSA is generally caused by the blocking of the airway. In the last few years, pulse transit time has been used to estimate a continuous signal of blood pressure if calibrated against a regular cuff-based blood pressure assessment at the beginning of the recording 6. A microphone attached to the trachea is used to document snoring and other noises during sleep, such as speaking [24].

A new wearable respiration monitoring system is introduced by Ishida et al which is attached to a shirt, consists of a piezoelectric sensor, a low-power microcontroller, EEPROM and a 2.4 GHz low-power transmitting mobile phone (PHS). The piezoelectric sensor is installed inside the shirt and closely contacts the patient's chest. The low frequency components of body movements recorded by the sensor are mainly generated by respiration. The microcontroller sequentially stores the movement signal to the EEPROM for 5 minutes and detects, by time-frequency analysis, whether the patient has breathed during that time. When the patient is apneic for 10 seconds, the microcontroller sends the recorded respiration waveform during and one minute before and after the apnea directly to the hospital server computer via the mobile phone [25].

2.3.3 Non-contact Detection Techniques:

A full wireless recording of sleep, respiration, and heartbeat has been developed as well. The first sensor systems which used foils in the bed to monitor sleep were used in Finland. Alihanka and Vaahtoranta were among the first to use this technology based on electrostatic effects with pressure-sensitive foils underneath a bed blanket in order to record sleep, heart rate, and respiration during sleep without any contact with the patient being investigated.

ApneaApp is a contactless solution developed by Rajalakshmi et al for detecting sleep apnea events by monitoring the minute chest and abdomen movements caused by breathing on smartphones. The system works with the phone away from the subject and simultaneously identify and track the fine-grained breathing movements from multiple subjects by transforming the phone into an active sonar system that emits frequency-modulated sound signals and listens to their reflections. They have developed algorithms that identify various sleep apnea events including obstructive apnea, central apnea, and hypopnea from the sonar reflections. [26] but failed to identify many hypopnea events accompanied with snoring properly. Other contactless technology is using infrared cameras but its computationally difficult, privacy concern and efficiency decreases during apnea event compared to normal breathing and movement

Kaiyin et al. developed and validated a vision-based non-contact monitoring system to estimate respiratory rate and heart rate during sleep using infrared camera. But, the proposed method for respiratory rate estimation is more accurate during normal breathing while asleep compared to wakefulness and respiratory events during sleep. In this study, an algorithm based on motion analysis of infrared video recordings was validated. Its computationally difficult, privacy concern and efficiency decrease during apnea event compared to normal breathing and movement [27].

A non-contact physiological radar monitoring system (PRMS) is introduced by Mehran Baboli [28] for sleep disorder monitoring. This PRMS utilizes continuous-wave Doppler radar and a real-time algorithm which recognizes paradoxical breathing to diagnose OSA and hypopnea. The PRMS was integrated with a standard PSG system to evaluate the efficacy for supplementing or replacing a standard PSG test for some applications. A clinical study was carried out using the PRMS on 10 subjects with known sleep apnea. In this study, the PRMS accurately diagnosed the occurrence of either an OSA or hypopnea event but was less effective for differentiating between them.

2.4 Machine Learning:

The name machine learning was coined in 1959 by Arthur Samuel. Tom M. Mitchell provided a widely quoted, more formal definition of the algorithms studied in the machine learning field: "A computer program is said to learn from experience E with respect to some class of tasks T and performance measure P if its performance at tasks in T, as measured by P, improves with experience E"[29]. This definition of the tasks in which machine learning is concerned offers a fundamentally operational definition rather than defining the field in cognitive terms. Most of us are unaware that we already interact with Machine Learning every single day. Every time we Google something, listen to a song or even take a photo, Machine Learning is becoming part of the engine behind it, constantly learning and improving from every interaction. It's also behind world-changing advances like detecting cancer, creating new drugs and self-driving cars.

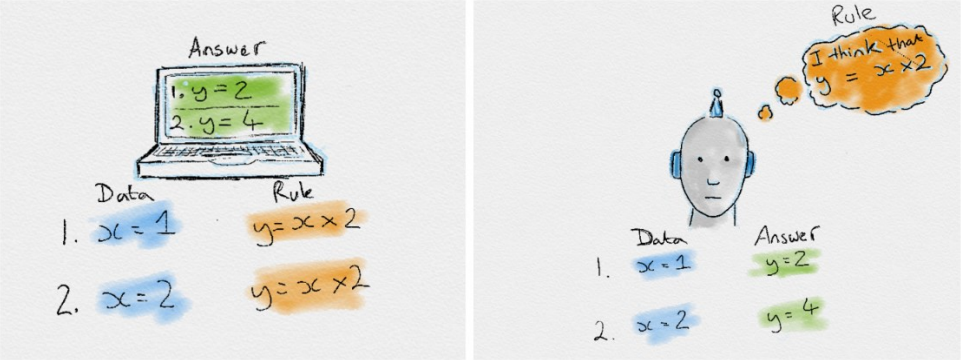

Fig 2.3: Pictorial representation of comparison of Traditional programming to Machine Learning [30]

Machine learning is an application of artificial intelligence (AI) that provides systems the ability to automatically learn and improve from experience without being explicitly programmed. Machine learning focuses on the development of computer programs that can access data and use it learn for themselves. The process of learning begins with observations or data, such as examples, direct experience, or instruction, in order to look for patterns in data and make better decisions in the future based on the examples that we provide. The primary aim is to allow the computers learn automatically without human intervention or assistance and adjust actions accordingly [31].

Resurging interest in machine learning is due to the same factors that have made data mining and Bayesian analysis more popular than ever. Things like growing volumes and varieties of available data, computational processing that is cheaper and more powerful, and affordable data storage. All these things mean it's possible to quickly and automatically produce models that can analyze bigger, more complex data and deliver faster, more accurate results – even on a very large scale. And by building precise models, an organization has a better chance of identifying profitable opportunities or avoiding unknown risks.

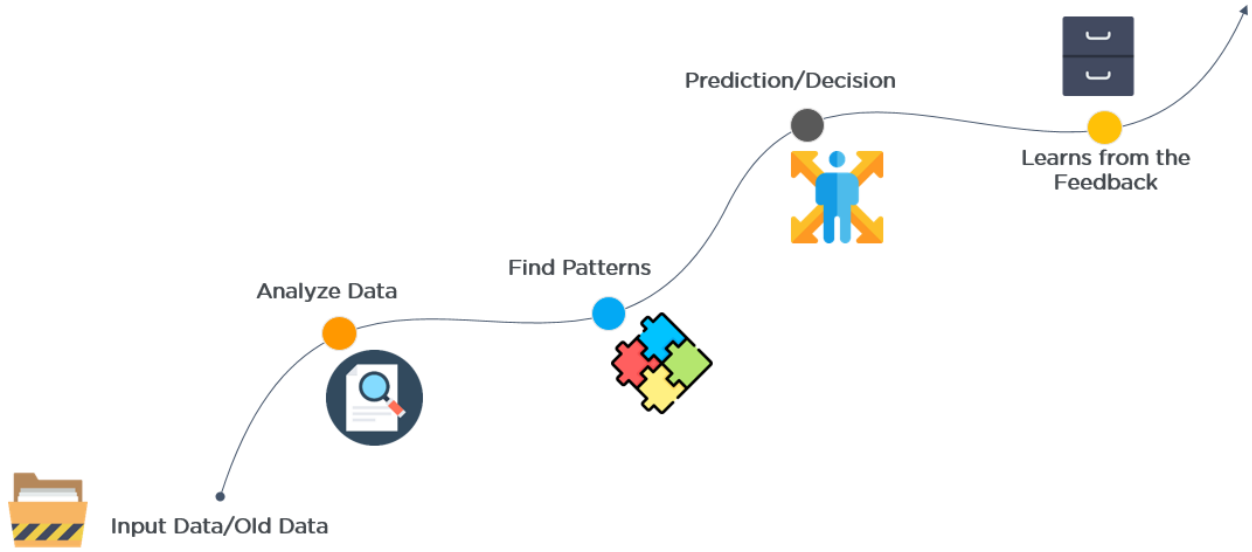

Fig 2.4: Working Procedure of Machine Learning in simple steps

Machine learning approaches in particular can suffer from different data biases. A machine learning system trained on current customers only may not be able to predict the needs of new customer groups that are not represented in the training data. When trained on man-made data, machine learning is likely to pick up the same constitutional and unconscious biases already present in society [32] Language models learned from data have been shown to contain human-like biases [33] Concern for fairness in machine learning, that is, reducing bias in machine learning and propelling its use for human good is increasingly expressed by artificial intelligence scientists, including Fei-Fei Li, who reminds engineers that "There's nothing artificial about AI...It's inspired by people, it's created by people, and—most importantly—it impacts people. It is a powerful tool we are only just beginning to understand, and that is a profound responsibility" [34].

2.4.1 Machine Learning Algorithms:

Two of the most widely adopted machine learning methods are supervised learning and unsupervised learning – but there are also other methods of machine learning. Here's an overview of the most popular types.

Supervised learning: These algorithms are trained using labeled examples, such as an input where the desired output is known. For example, a piece of equipment could have data points labeled either “F” (failed) or “R” (runs). The learning algorithm receives a set of inputs along with the corresponding correct outputs, and the algorithm learns by comparing its actual output with correct outputs to find errors. It then modifies the model accordingly. Through methods like classification, regression, prediction and gradient boosting, supervised learning uses patterns to predict the values of the label on additional unlabeled data.

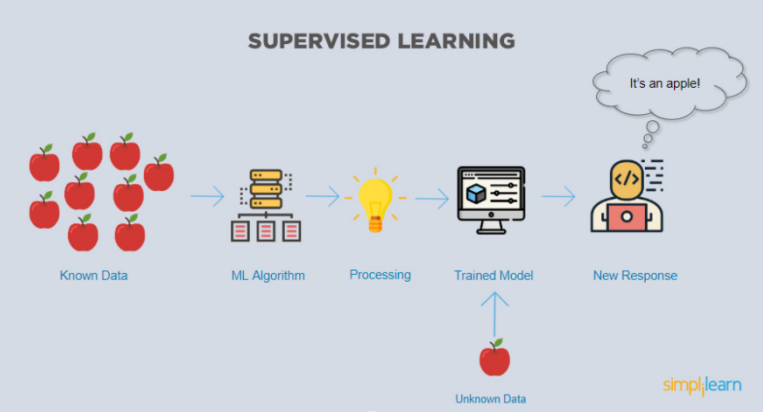

Fig 2.5: Pictorial representation of Supervised learning

Unsupervised learning: The algorithm is used against data that has no historical labels. The system is not told the "right answer." The algorithm must figure out what is being shown. The goal is to explore the data and find some structure within. Unsupervised learning works well on transactional data. For example, it can identify segments of customers with similar attributes who can then be treated similarly in marketing campaigns. Or it can find the main attributes that separate customer segments from each other. Popular techniques include self-organizing maps, nearest-neighbor mapping, k-means clustering and singular value decomposition. These algorithms are also used to segment text topics, recommend items and identify data outliers.

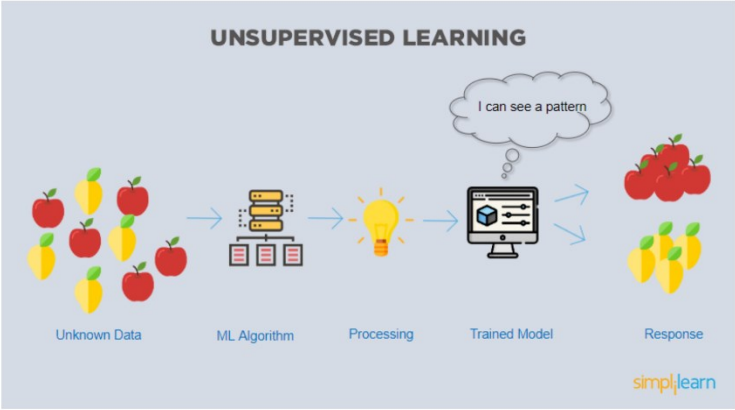

Fig 2.6: Pictorial representation of Unsupervised learning

Semi-supervised learning: These algorithms are used for the same applications as supervised learning. But it uses both labeled and unlabeled data for training – typically a small amount of labeled data with a large amount of unlabeled data (because unlabeled data is less expensive and takes less effort to acquire). This type of learning can be used with methods such as classification, regression and prediction. Semi-supervised learning is useful when the cost associated with labeling is too high to allow for a fully labeled training process. Early examples of this include identifying a person's face on a web cam.

Reinforcement learning: These algorithms are often used for robotics, gaming and navigation. With reinforcement learning, the algorithm discovers through trial and error which actions yield the greatest rewards. This type of learning has three primary components: the agent (the learner or decision maker), the environment (everything the agent interacts with) and actions (what the agent can do). The objective is for the agent to choose actions that maximize the expected reward over a given amount of time. The agent will reach the goal much faster by following a good policy. So, the goal in reinforcement learning is to learn the best policy.

Machine learning enables analysis of massive quantities of data. While it generally delivers faster, more accurate results in order to identify profitable opportunities or dangerous risks, it may also require additional time and resources to train it properly. Combining machine learning with AI and cognitive technologies can make it even more effective in processing large volumes of information.

2.4.2. K Nearest Neighbor (KNN):

K-Nearest Neighbors (KNN) is one of the simplest supervised algorithms used in Machine Learning for regression and classification problem. KNN algorithms use data and classify new data points based on similarity measures (e.g. distance function). Classification is done by a majority vote to its neighbors. The data is assigned to the class which has the nearest neighbors. As the number of nearest neighbors is increased, the value of k, accuracy might increase. The KNN algorithm assumes that similar things exist in proximity. In other words, similar things are near to each other like "Birds of a feather flock together." The KNN algorithm hinges on this assumption being true enough for the algorithm to be useful. It is commonly used for its easy of interpretation and low calculation time.

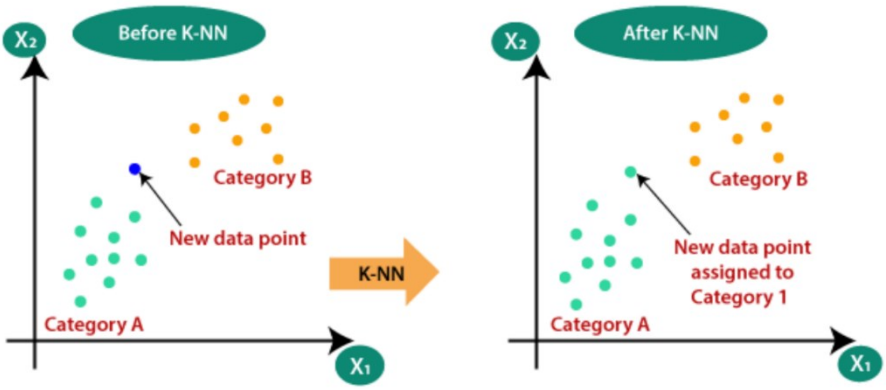

Fig 2.7: Working procedure of KNN algorithm. From training data set, KNN categorizes data set and on base of k value categorize the new data

KNN is an algorithm that is considered both non-parametric and an example of lazy learning. Non-parametric means that it makes no assumptions. The model is made up entirely from the data given to it rather than assuming its structure is normal. Lazy learning means that the algorithm makes no generalizations. This means that there is little training involved when using this method. Because of this, all the training data is also used in testing when using KNN. To select the K that's right for data, the KNN algorithm need to be run several times with different values of K and that value of K is chosen that reduces the number of errors encountered while maintaining the algorithm's ability to accurately make predictions when it's given data it hasn't seen before.

The K-NN working procedure of KNN computation model (algorithm) can be explained in certain steps. At first, the number K of the neighbors is selected. On basis of that number of

neighbors, K the Euclidean distance is calculated. As per calculation Euclidean distance, K nearest neighbors are taken. The data points in each category is counted among these k-neighbors. For new data point, the number of the neighbor for each category is calculated. The new data is categorized into the category which number of the neighbor is maximum for it. That's how KNN model works. To use KNN algorithm to get result, there are some steps to make data set ready. These steps to implement the K-NN algorithm are shown below:

- Data Pre-processing step
- Fitting the K-NN algorithm to the Training set
- Predicting the test result
- Test accuracy of the result (Creation of Confusion matrix)
- Visualizing the test set result

KNN is often used in simple recommendation systems, image recognition technology, and decision-making models. It is the algorithm companies like Netflix or Amazon use in order to recommend different movies to watch or books to buy. These companies will apply KNN on a data set gathered about the movies watched or the books bought on their website. These companies will then input available customer data and compare that to other customers who have watched similar movies or bought similar books. This data point will then be classified as a certain profile based on their past using KNN. The movies and books recommended will then depend on how the algorithm classifies that data point. [33]

2.4.3. Support Vector Machine (SVM):

Support-vector machines (SVM), are supervised learning models with associated learning algorithms that analyze data used for classification and regression analysis. SVM is a discriminative classifier formally defined by a separating hyperplane. In other words, given labeled training data (supervised learning), the algorithm outputs an optimal hyperplane which categorizes new examples. In two-dimensional space this hyperplane is a line dividing a plane in two parts where in each class lay in either side. The objective of the SVM algorithm is to find a hyperplane in an N-dimensional space (N — the number of features) that distinctly classifies the data points. To separate the two classes of data points, there are many possible hyperplanes that could be chosen. The objective is to find a plane that has the maximum margin, i.e the maximum distance between data points of both classes. Maximizing the margin distance provides some reinforcement so that future data points can be classified with more confidence. [34]

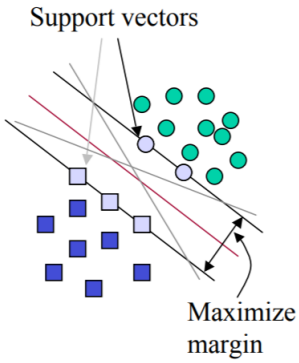

Fig 2.8: Pictorial representation of how SVM algorithm categorize data using hyperplane in 2D space

Support vector machine is highly preferred by many as it produces significant accuracy with less computation power. Hyperplanes are decision boundaries that help classify the data points. Data points falling on either side of the hyperplane can be attributed to different classes. Also, the dimension of the hyperplane depends upon the number of features. If the number of input features is 2, then the hyperplane is just a line. If the number of input features is 3, then the hyperplane becomes a two-dimensional plane. It becomes difficult to imagine when the number of features exceeds 3.

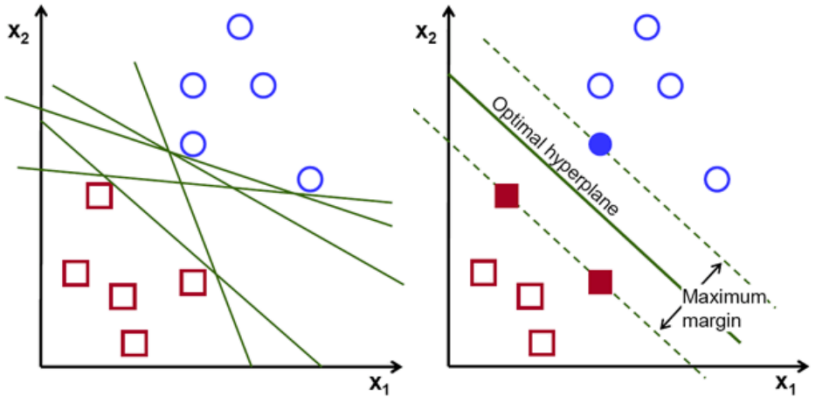

Fig 2.9: Representation of Support vector

Support vectors are data points that are closer to the hyperplane and influence the position and orientation of the hyperplane. Support vectors maximize the margin of the classifier. Deleting the support vectors will change the position of the hyperplane. These are the points that help us build SVM.

The advantages of support vector machines, its effective in high dimensional spaces and still effective in cases where number of dimensions is greater than the number of samples. It uses a subset of training points in the decision function (called support vectors), so it is also memory efficient. SVM is versatile which means different Kernel functions can be specified for the decision function. Common kernels are provided, but it is also possible to specify custom kernels. The disadvantages of support vector machines include, if the number of features is much greater than the number of samples, avoid over-fitting in choosing Kernel functions and regularization term is crucial. SVMs do not directly provide probability estimates, these are calculated using an expensive five-fold cross-validation (see Scores and probabilities, below).

2.5 Summary:

This chapter summarized some of the contact and non-contact sleep apnea detection and techniques including PSG, smartphone use, IR-based sensor and radar and Machine learning algorithms. PSG is reliable but its uncomfortable, expensive and can't be used for night to night monitoring. Consequently, numerous alternative sleep monitoring technologies have been developed to overcome the disadvantages of full night PSG recording, using reduced number of sensors and allowing for at-home recording [35]. Most consumer technologies come at a cost of reduced accuracy and cannot be used as a stand-alone solution [36], while most clinical modalities still require multiple sensors and a board-certified sleep medicine specialist [37]. Moreover, an attachment of multiple sensors could potentially be inconvenient during sleep. Various contactless technologies were explored for overnight respiratory rate and/or heart rate monitoring including applications of radar [38], WiFi [39], audio recording [40], pressure sensors [41], depth cameras [42], thermal cameras [43], and infrared cameras [44]. Machine learning is a fast-growing trend in the health care industry, thanks to the advent of wearable devices and sensors that can use data to assess a patient's health in real time. The technology can also help medical experts analyze data to identify trends or red flags that may lead to improved diagnoses and treatment.

Chapter -3

Doppler Radar System

3.1 Radar:

The term Radar is derived from the original name given to this technique that was Radio Detection And Ranging [45]. Pulses of electromagnetic waves (EM) are generated by the transmitter and sent to a radiating antenna which usually focuses the EM wave energy into a beam towards the target [46]. The received signal is received by the same antenna (duplex) or a different antenna and is sent to the receiver which proceeds signal processing system (Figure 3.1). After the signal processing, the results are displayed. The radar is designed to search and detect the target of interest and to determine certain target parameters [46].

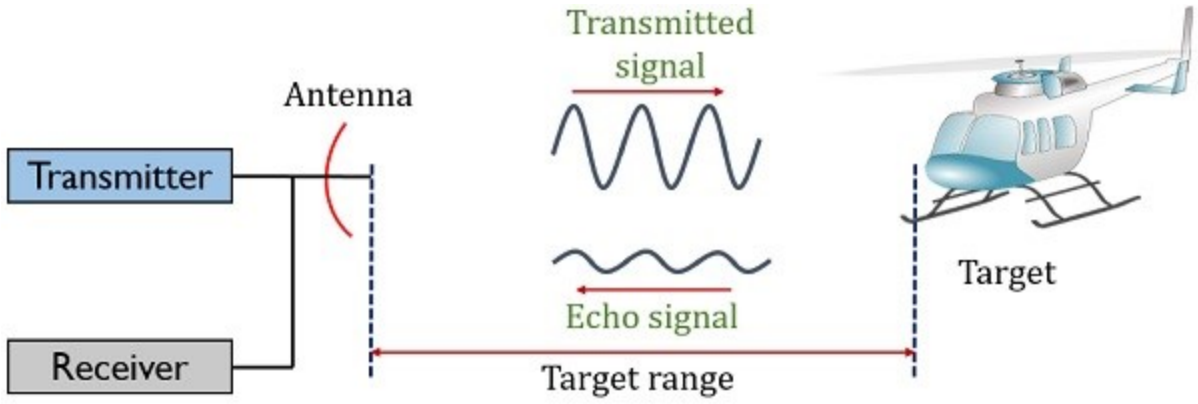

Fig 3.1: Block diagram of a radar system showing antenna

Determination of radar range is very crucial in designing or evaluating a radar's performance. A very simplified range equation is given below:

$$R_{\max} = \left[\frac{P_t A_e G \sigma}{(4\pi)^2 s\min}\right]^{1/4} \quad (3.1)$$

Here, Pt = transmitted power, W

Ae = Antenna effective aperture, m2

G = Antenna gain,

σ = Radar cross section of the target, m2

$Smin$ = Minimum detectable signal, W

The parameters of this maximum range equation can be designed; however, the designer cannot control the target's radar cross section. To achieve long range the transmission power should be higher. For short range operation, the transmission power can be kept considerably low; the energy radiation not necessarily has to be a very narrow beam, a small aperture antenna can receive the echo energy. All these design parameters present the trade-offs between having a large range versus small power small sized radar system [46].

3.2 Doppler Radar:

The Austrian physicist Christian Doppler introduced the idea of 'doppler radar' in 1842. The Doppler effect (or the Doppler shift) is the change in frequency of a wave in relation to an observer who is moving relative to the wave source. A Doppler radar is a specialized radar that uses the Doppler effect to produce velocity data about objects at a distance. It does this by bouncing a microwave signal off a desired target and analyzing how the object's motion has altered the frequency of the returned signal.

Pulse radar emits short and powerful pulses and in the silent period receives the echo signals. It is important to understand the principle of pulse Doppler radar because it leads us to the understanding of phase modulation. Radial velocity is required for pulse-Doppler radar operation. Pulse radar sends out pulse RF with some interval. As the target moves between each transmit pulse the return signal will undergo a phase change from pulse to pulse, thus creating Doppler modulation. The phase shift of the returning pulse can be measured by –

$$\Delta\emptyset = \frac{4\pi(v\Delta t)}{\lambda} \tag{3.2}$$

Where, $\Delta\emptyset$ = phase shift

λ = Wavelength of the transmitted signal

v = Velocity of the moving object

Δt = Time interval between two pulses

Consider a case where a target has a low-frequency oscillating motion on a fixed nominal distance from radar. The target is neither going away nor coming towards the radar. So, the net velocity of the target is 0. In short distance application, a target having a net 0 velocity the Doppler frequency shift measurement is hard to produce good results, it will be almost 0 which can be realized analyzing equation 3.2. We may use phase modulation information instead of Doppler frequency shift to track the low-frequency motion of the slow-moving torso of the target. If a continuous wave radar is used instead of pulse radar,

$$v(\Delta t) = x(t) \tag{3.3}$$

Then equation 3.2 becomes: $$\Delta\emptyset = \frac{4\pi(x(t)}{\lambda} \tag{3.4}$$

where, x(t) is time varying position of the target.

Continuous wave Doppler radars are the kind that transmits RF signal towards the target ceaselessly. This kind of radar has some advantages over pulse radar. Continuous wave radar can completely produce the motion of a target within the environment of a stationary clutter. This type of radars has many applications in the field of biomedical science.

3.3 Doppler radar in Physiological Monitoring:

In late 1970, the use of microwave Doppler radar for monitoring respiratory and cardiac movements was first introduced but measured separately while breath-hold was required [57 of 2.1 of Amy's thesis]. In 1975 James Lin measured respiration signal of rabbit and human from a 30 cm distance using X-band sweep oscillator equipped with a rectangular horn antenna. He and his team continued research on using the microwave for detecting apnea noninvasively and was published in 1977. From mid-1980 to late 1990 radar transceiver was developed that incorporated analog and digital signal processing to separate small heart signal from the much larger respiration signal, so the subject need not to hold the breath thus both heart rate and respiration rate can be measured simultaneously [47] [48]. These transceivers were used for the detection of heart and respiration rates of persons in rubble, person behind wall and Olympic athletes. Chan and Lin [47] combined analog amplification and filtering for separation of heart and respiration rates with 8-bit quantization and digital signal processing to detect heart and respiration rates. An automatic clutter-cancellation circuit was developed by Chuang et al facilitate measurements of heart and respiration through seven layers of brick [49]. A quadrature receiver was used to avoid phase-demodulation null points by J. Seals et al [50]. Matsui et al have proposed Doppler radar vital signs monitoring to detect hypovolemic states and shock in persons under rubble or in biochemical hazard conditions that could pose danger to health care providers [51] [52].

A modified wireless LAN PCMCIA card was used to detect heart and respiration by Boric-Lubecke et al [53] and a module that combines the transmitted and reflected signals from any wireless communication device, such as a cordless telephone, was used to detect heart and respiration by Lubecke et al [54]. Quadrature Doppler radars were developed, and different modulation techniques were proposed for accurate respiration and heart signal measurement. Techniques were also developed in last decades to compensate for distortion such as AC coupling distortion, I/Q channel imbalances, random body motion cancellation. Hybrid FMCW-interferometer radar was proposed for precise 2-D positioning and life activities surveillance. The proposed hybrid radar works in the 5.8 GHz ISM band with a 160 MHz bandwidth [11 of Ashik]. Using this technology to directly connect Doppler measurement of heart and respiration rate to health care providers has been proposed [55].

Additionally, ultra-wideband radar has been used for measurement of heart and respiration rates. Using 0.4 W pulses and 1 GHz central frequency, heart rates were detected through 1 m of air and a 0.4 m brick wall [56] and respiration was measured at up to 5 m [57].

3.4 Doppler radar Topology:

Recent developments in non-invasive radar measurement of small-scale motion offer great potential for indoor activity classification in applications such as health diagnostics, health monitoring, surveillance, product tracking product, occupancy sensing, and animal research [58] [59]. Combined with wireless body area networks and indoor localization technology, measurement, and recognition of biological motion patterns will shape the future of home and workplace security, safety and comfort [60].

In a Doppler radar for monitoring cardiopulmonary motion, the associated noise basically residual phase noise and baseband noise. So, the receiver should maximize the ability to differentiate between physiological data and these noises. There are trade-offs between several parameters signal to noise ratio, cost, weight, size, bandwidth, and some design choices at system architecture levels.

3.4.1 Continuous-Wave Radar:

A continuous wave radar system transmits and receives a very narrow bandwidth signal. CW radar uses the Doppler Effect to detect a moving target. It transmits a continuous wave signal with constant energy. The frequency of the received signal scattered back from the target has a shift which is proportional to the target velocity.

The rate change of the phase as a result of moving target (i.e variable R) is given by:

$$\omega_d = \frac{d\phi}{dt} = \frac{4\pi\, dx(t)}{\lambda\, dt} = \frac{4\pi v(t)}{\lambda} = 2\pi f_d \tag{3.5}$$

Where f_d is the doppler frequency shift. It can be calculated from the equation below:

$$f_d = \frac{\omega_d}{2\pi} = \frac{2v(t)}{\lambda} = \frac{2f_t v(t)}{c} \tag{3.6}$$

Here, f_t is frequency of transmitted signal and c is velocity of wave propagation.

In continuous wave radar consists of a signal source that is used for both transmitting and receiving and either be a homodyne or heterodyne receiver. Because of its simple topology, it doesn't need a transmit/receiver switch as opposed to pulsed radar system. The narrow band nature of CW radar made possible use of simple filter at each stage of the receiver. Also, the signal processing is straightforward if velocity or displacement is desired. The main system level advantage is it can measure any velocity of target at any range, which is not possible is pulse or other systems. A major drawback of CW radar is constant transmitting made it hard to separate reflections temporally. A portion of transmitting signal leaks from transmitter to receiver through coupling or through antenna. Also, the signal reflected from clutter results in dc offset and low-frequency noise if not eliminated before signal is detected [61]. Additionally, clutter reflects some of the signal and its noise sidebands back to the receiver, adding to the signal power at the transmit frequency due to leakage. These unwanted signals results in a dc offset and low frequency noise if they are not eliminated before the signal is detected.

3.4.2 Pulse Radar:

A pulsed radar system switches between transmitting and receiving, and the signal has a somewhat wider bandwidth because of the pulses. The waveform of the transmitted signal can be described mathematically as:

$$s(t) = A(t) \cdot \sin[2\pi f(t) \cdot t + \phi(t)] \tag{3.7}$$

The function A(t) is a variation of the amplitude in the function of time t – i.e. an amplitude modulation. In the simplest case, the transmitter is for a short time switched on (for the time τ) and remains in the rest of the time in the "off position". The function of time is then determined by the pulse repetition frequency and the duty cycle. Since the radar returns are subject to various losses, an actual amplitude modulation makes little sense except for just this switching

function (On/off keying). It is typically used in situations where the return signal is much smaller than the transmitted one or when the peak power of the transmitted signal is much higher than the average. Important distinguishing feature to other radar method is the necessary time control of all processes inside the pulse radar.

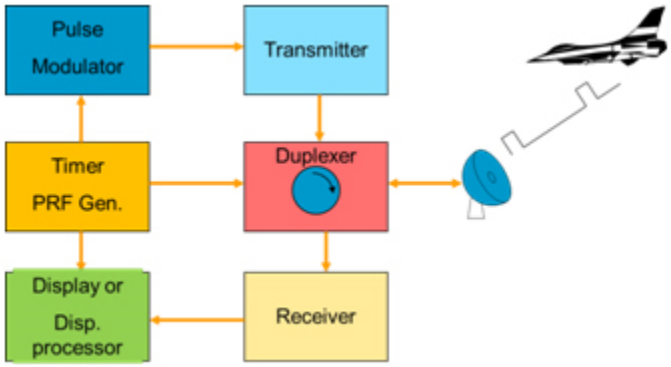

Fig 3.2: Block diagram of a pulse radar system

A major advantage of pulse radar is the ability to instantaneously measure target range. A transceiver with a pulse repetition period longer than the round-trip path length transmits a burst of energy and then listens for echoes between transmissions. The leakage from the transmitter and strong echoes from short range clutter are separated temporally from the weaker echoes of long-range targets, this is the main advantage of pulsed radar over CW radar. Another major advantage is the ability to instantaneously measure target range.

The leakage from transmitter strong echoes from closer clutter can be separated temporally from weak echoes of long-range target in pulsed radar system compared to CW radar. But, in Doppler monitoring of heart and respiration motion the target is typically at same or shorter range than the nearest clutter, so pulsed radar system's advantage is only the elimination of leakage. Range measurement also do not help in Doppler monitoring of heart and respiration motion. So, CW radar system is used for Doppler monitoring as its simplest topology with only single oscillator and its extreme narrow single bandwidth avoids interferences and ease filtering requirements [61]. Also, the goal of the measurement is target motion rather than distance of the target so pure CW radar system is ideal.

3.4.3 Single Channel Receiver:

In a single-channel receiver, shown in Fig. 3.2, the phase-modulated RF signal is directly mixed with the single tone local oscillator carrier. Since the transmitted RF signal and the reference tones are generated from the same oscillator, the phase noise associated with each component is correlated. This results in a reduced phase-noise in the signal at the output of the mixer. The signal at the RF input of the mixer is represented as:

$$RF_{in}(t) = A_{RF}\cos\left(\omega_0 t - \frac{4\pi}{\lambda}x(t) + \phi_n(t - t_0) + \phi_{RF}\right) \tag{3.8}$$

where A_{RF} is the amplitude, $\phi_n(t-t_o)$ is the phase noise delayed by the round trip traveled by the carrier, and the constant phase is:

$$\phi_{RF} = -\frac{4\pi}{\lambda}R_0 + \phi_{in} + \emptyset o \tag{3.9}$$

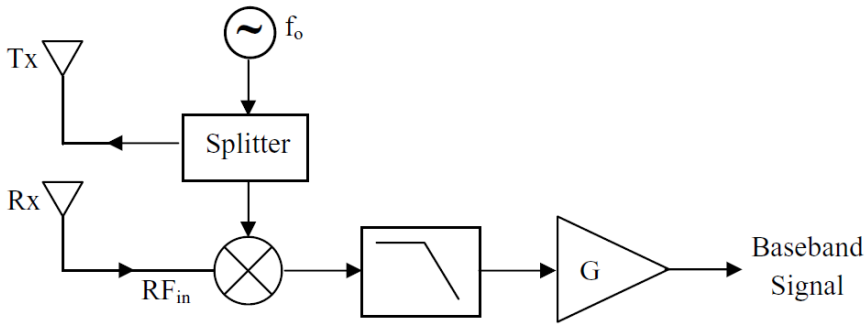

Fig 3.3: Single channel receiver configuration

On the other hand, the local oscillator carrier can be represented as:

$$S_{LO}(t) = A_{Lo}\cos(\omega_0 t + \phi_n(t) + \phi_{L0}) \tag{3.10}$$

where A_{LO} and ϕ_{LO} are the amplitude and initial phase at the Lo input of the mixer, respectively. Mixing of the RF and Lo signals results in two components, one is at twice the carrier frequency and the other is a suppressed carrier baseband signal. At the output of the low pass filter, the baseband signal is represented as:

$$S_{BB} = A\cos\left(\frac{4\pi}{\lambda}x(t) + \phi_{tot} + \Delta\phi(t)\right) \tag{3.11}$$

where A is the amplitude, $\phi_{tot}=\phi_{LO}-\phi_{RF}$ is the total constant phase, and $\Delta\phi(t)=\phi_n(t)-\phi_n(t-t_o)$ is the residual phase noise. The design of single channel receiver is simple and requires minimum hardware but the sensitivity of the demodulated signal is directly dependent on the constant phase ϕ_{tot} of the baseband signal. The constant phase is in turn dependent on the target range. When ϕ_{tot} equals to an odd multiple of $\pi/2$, the baseband signal becomes:

$$S_{BB} = A\cos\left(\frac{4\pi}{\lambda}x(t) + \Delta\phi(t)\right) \tag{3.12}$$

If the torso displacement magnitude is small with respect to wavelength, the small angle approximation holds and:

$$S_{BB} = \mathrm{A}\left(\frac{4\pi}{\lambda}x(t) + \Delta\phi(t)\right) \tag{3.13}$$

This condition is referred to as "optimum point" and corresponds to maximum sensitivity where the baseband signal is directly proportional to the displacement of the torso. On the other hand, when ϕ_{tot} equals to a multiple of π, the small angle approximation leads to:

$$S_{BB} = \frac{\mathrm{A}}{2}\ [\left(\frac{4\pi}{\lambda}x(t) + \Delta\phi(t)\right)\text{^}2] \tag{3.14}$$

The squaring of the torso displacements leads to minimum sensitivity and this condition is referred to as "null point". For other values of ϕ_{tot}, the baseband signal will lie between null and optimum conditions. Since, ϕ_{tot} is a function of the round-trip phase shift of the propagating wave, the sensitivity of the single channel receiver depends on the target range [35].

3.4.4 Quadrature Receiver:

The constant phase values corresponding to optimum and null points differ by $\pi/2$. Therefore, the dependence of phase demodulation accuracy on the target range can be overcome by obtaining the baseband signal in form of two components in quadrature. This is implemented by adding a channel consisting of a mixer, filter, and amplifier, as shown in Fig. 3.3. The RF signal is split into two components, one for each channel, while the local oscillator is split into in-phase and quadrature components. The 90-degree splitter is usually a branch line coupler that delivers two components equal in amplitude but offset by $\pi/2$. If the leading component is considered as in phase, the local oscillator signals at the input of the mixer are:

$$I_{LO}(t) = A_{Lo}\cos(\omega_0 t + \phi_n(t) + \phi_{L0}) \tag{3.15}$$

$$Q_{LO}(t) = A_{Lo}\cos(\omega_0 t + \phi_n(t) + \phi_{L0}) \tag{3.1}$$

where I_{LO} and Q_{LO} are the in-phase and quadrature components, respectively.

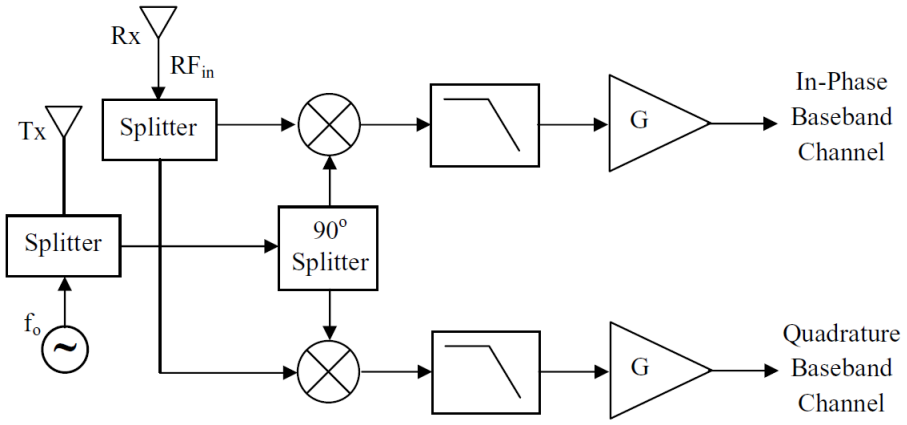

Fig 3.4: Quadrature receiver configuration

Mixing each signal with RF_{in} and filtering out the high frequency band will lead to two baseband signals that are also in quadrature and expressed as:

$$I_{BB} = A\cos\left(\frac{4\pi}{\lambda}x(t) + \phi_{tot} + \Delta\phi(t)\right) \tag{3.17}$$

$$Q_{BB} = A\cos\left(\frac{4\pi}{\lambda}x(t) + \phi_{tot} + \Delta\phi(t)\right) \tag{3.18}$$

I_{BB} and Q_{BB} are referred to as the I-channel and Q-channel, respectively. Each channel is filtered, amplified and digitally acquired independently. The digital signal processing stage then applies the demodulation technique, in this case, the center estimation algorithm. On the complex I-Q plot, the baseband signal forms an arc that has a radius A and which scans an angle proportional to the torso displacement, $x(t)$. The position of the arc can be anywhere in the four quadrants or on the axes depending on the value of ϕ_{tot}. In the time domain, the relation between I_{BB} and Q_{BB} with respect to each other and with respect to the torso movement is a function of the location of the arc on the complex I-Q plane.

Quadrature receiver can avoid the phase demodulation null points with range that makes heart rate detection less accurate at some ranges. By choosing the larger of the two signals, which should be closer to the optimal phase demodulation point, through direct phase demodulation, or by combining the signals with technique. However, a quadrature receiver means two receiver which is more costly, take more space in die and makes integrated circuit more complex to fabricate. For this work, a CW wave radar with quadrature channel receiver is selected.

3.4.5 Homodyne Receiver:

The simplest phase detector involves mixing the received signal with a signal at the same frequency as its carrier, so that the RF frequency is converted directly to baseband. A direct-conversion receiver (DCR), also known as homodyne, synchro-dyne, or zero-IF receiver, is a radio receiver design that demodulates the incoming radio signal using synchronous detection driven by a local oscillator whose frequency is identical to, or very close to the carrier frequency of the intended signal. (Homodyne is sometimes used to describe a system where the local oscillator is synchronized in phase with the incoming signal [62]).

Homodyne detection is more readily applicable to velocity sensing. The main advantage of a homodyne receiver is that it does not suffer the image problem as the incoming RF signal is down-converted directly to baseband without any IF stage. Another advantage of the homodyne architecture is its simplicity. The advantage of the homodyne receiver is that it is low-cost. The receiver used in a police radar gun is a homodyne receiver.

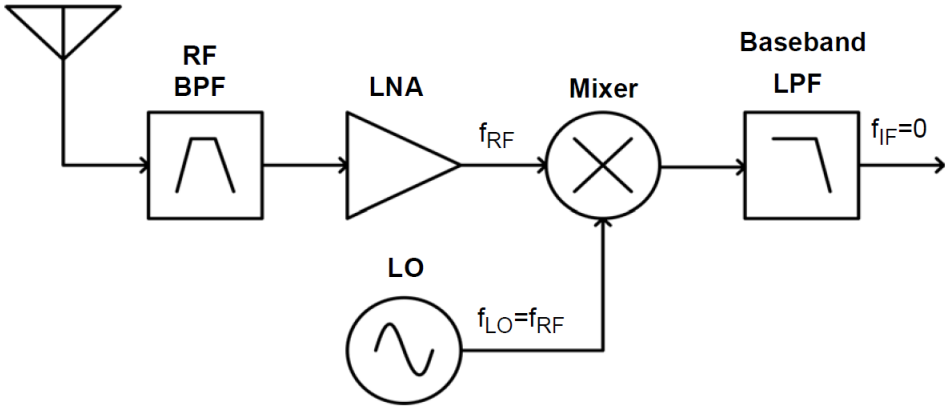

Fig 3.5: Direct conversion or Homodyne receiver architecture

In a homodyne receiver, the received signal is sometimes bandpass filtered to remove noise and amplified with an LNA to decrease the receiver noise figure. The signal is then mixed with an LO at the same frequency as its carrier, converting the signal to baseband. Depending on the modulation of the signal, this may complete the demodulation, or an additional detector may be required. In a homodyne system, both sidebands of the signal are converted to the same frequency space at baseband. Because this problem is analogous to the image frequency problem in a heterodyne receiver, it is known as self-imaging problem.

3.4.6 Heterodyne Receiver:

Heterodyning is a signal processing technique invented by Canadian inventor-engineer Reginald Fessenden that creates new frequencies by combining or mixing two frequencies [[1][2][3] of wiki]. Heterodyning is used to shift one frequency range into another, new one, and is also involved in the processes of modulation and demodulation [63] [64]. The two frequencies are combined in a nonlinear signal-processing device such as a vacuum tube, transistor, or diode, usually called a mixer.[63] In the most common application, two signals at frequencies f1 and f2 are mixed, creating two new signals, one at the sum f1 + f2 of the two frequencies, and the other at the difference f1 − f2.[64] These frequencies are called heterodynes. Typically, only one of the new frequencies is desired, and the other signal is filtered out of the output of the mixer.

Heterodyning, also called frequency conversion, is used very widely in communications engineering to generate new frequencies and move information from one frequency channel to another. Besides its use in the super-heterodyne circuit found in almost all radio and television receivers, it is used in radio transmitters, modems, satellite communications and set-top boxes, radar, radio telescopes, telemetry systems, cell phones, cable television converter boxes and headends, microwave relays, metal detectors, atomic clocks, and military electronic countermeasures (jamming) systems.

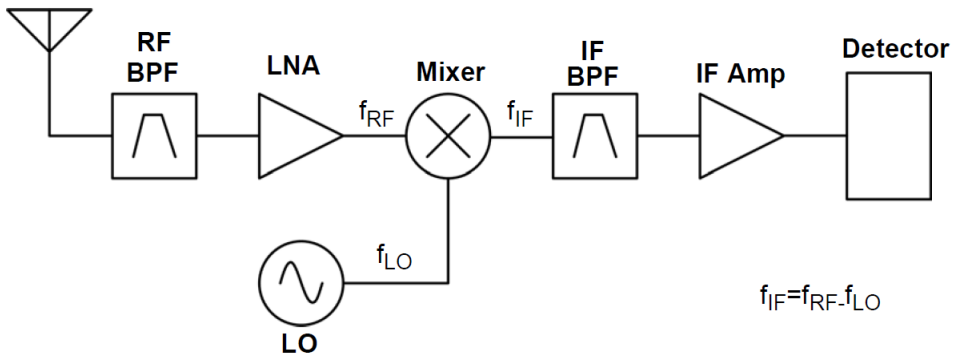

Fig 3.6: Typical heterodyne receiver architecture

In a heterodyne receiver, the input signal is amplified and filtered at RF, then mixed to an intermediate frequency (IF) where it is amplified in a tuned IF stage and filtered with high quality fixed bandpass filters before the signal is detected (which may involve mixing to baseband). The RF bandpass filter or pre-selector is designed to eliminate the image frequency, the undesired signal capable of producing the same IF as the desired signal produces when mixed with the LO. The low noise amplifier (LNA) decreases the receiver noise figure by increasing the signal power at the input before the rest of the receiver adds noise. The signal is then mixed with the LO to down convert it to the intermediate frequency. The IF bandpass filter is used to isolate the desired channel from neighborhood channels, so it is generally a high-quality complex filter. The IF amplifier is

often a gain-controlled amplifier that adjusts the signal to the appropriate amplitude for the detector. The detector varies depending on the modulation scheme and the type of information that is modulated. It may consist of down conversion to baseband, a differentiator, an envelope detector, a phase-locked loop, or other topologies.

The homodyne receiver is selected for the application of detecting physiological signal using Doppler radar due to its simplicity and its straightforward use as a phase detector. The information about the periodic target motion can be readily demodulated if this signal is multiplied by a local oscillator (LO) signal that is derived from the same source as the transmitted signal in a direct conversion architecture. Because the phase noise of the received signal is correlated with that of the LO, ignoring amplitude variations.

3.5 Doppler System Architecture:

Non-contact physiological monitoring is possible with Doppler radar. For this aim, Continuous wave microwave signal illuminates the human subject under measurement. A live human subject will have cardiopulmonary activity resulting in physiological motions. The skin surface on the chest wall will have small displacements with every heartbeat and breath. These small displacements contribute to variations in the roundtrip time of the received signal proportional to the subject's physiological motion. The received signal is compared to the transmitted signal using a frequency mixer which outputs the phase difference between the two signals. The phase difference is caused by variations in the roundtrip travel time of the signal which is proportional to the physiological motions of the subject.

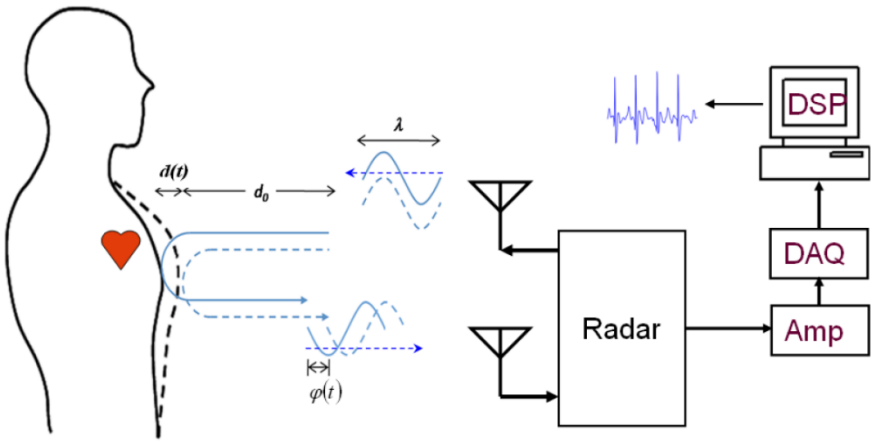

Fig 3.7: Principal of operation of Doppler radar and its main components [67]

Major components in the figure are the radar front end and antennas, baseband amplifiers, data acquisition system and digital signal processing. Microwave signal is generated in the radar front end and transmitted through the transmit antenna toward the subject. Reflected signal from the subject which is phase modulated due to patient's physiological motions is received using the receive antenna. The received signal is down converted from microwave region to DC (or near DC) and passes through amplifiers and data acquisition. Digital to analog conversion within the DAQ creates a digital version of the baseband radar signal which can be processed further using numerous DSP techniques.

For human physiological monitoring in this dissertation, quadrature channel Continuous-wave homodyne receiver is selected. CW radar system is used for Doppler monitoring as its simplest topology with only single oscillator and its extreme narrow single bandwidth avoids interferences and ease filtering requirements [61]. Also, the goal of the measurement is target motion rather than distance of the target so pure CW radar system is ideal. The homodyne receiver is selected for the application of detecting physiological signal using Doppler radar due to its simplicity and its straightforward use as a phase detector. The information about the periodic target motion can be readily demodulated if this signal is multiplied by a local oscillator (LO) signal that is derived from the same source as the transmitted signal in a direct conversion architecture. Quadrature receiver can avoid the phase demodulation null points with range that makes heart rate detection less accurate at some ranges.

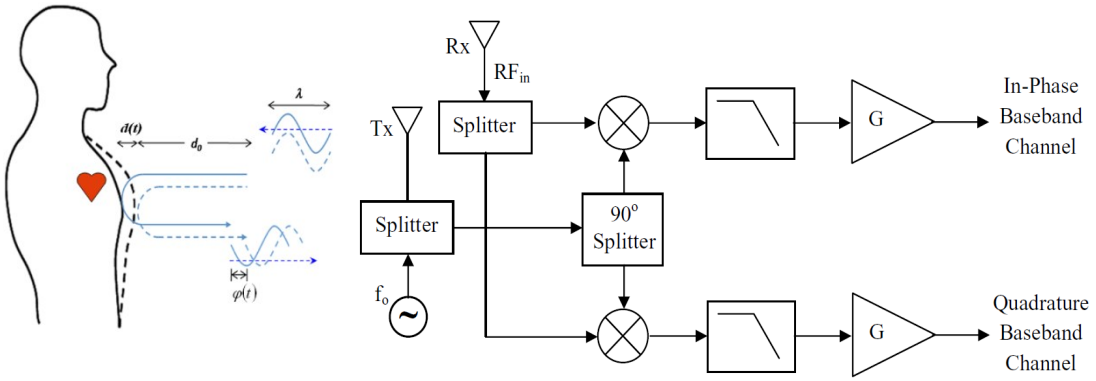

Fig 3.8: A quadrature Continuous wave Doppler radar system

The constant phase values corresponding to optimum and null points differ by $\pi/2$. Therefore, the dependence of phase demodulation accuracy on the target range can be overcome by obtaining the baseband signal in form of two components in quadrature. This is implemented by adding a channel consisting of a mixer, filter, and amplifier. The RF signal is split into two components, one for each channel, while the local oscillator is split into in-phase and quadrature components. The 90-degree splitter is usually a branch line coupler that delivers two components

equal in amplitude but offset by π/2. If the leading component is considered as in-phase, the local oscillator signals at the input of the mixer are:

$$I_{L0}(t) = A_{L0}\cos(\omega_0 t + \phi(t) + \phi_{L0}) \tag{3.19}$$

$$Q_{L0}(t) = A_{L0}\sin(\omega_0 t + \phi(t) + \phi_{L0}) \tag{3.20}$$

where I_{LO} and Q_{LO} are the in-phase and quadrature components, respectively.

Mixing each signal with RF_{in} and filtering out the high frequency band will lead to two baseband signals that are also in quadrature and expressed as:

$$I_{BB} = A\cos\left(\frac{4\pi}{\lambda}x(t) + \phi_{tot} + \Delta\phi(t)\right) \tag{3.21}$$

$$Q_{BB} = A\sin\left(\frac{4\pi}{\lambda}x(t) + \phi_{tot} + \Delta\phi(t)\right) \tag{3.22}$$

I_{BB} and Q_{BB} are referred to as the I-channel and Q-channel, respectively. Each channel is filtered, amplified and digitally acquired independently. The digital signal processing stage then applies the demodulation technique.

3.6 Demodulation Algorithm:

The in-phase and quadrature baseband signals are digitally acquired through an analog-to-digital converter. At the output of the converter, each signal is represented by a vector of data that can be processed in the digital domain. The processing algorithm is designed to extract the required information about the target, namely the rate of motion, the depth of motion and the effective radar cross section of the target. This section represents the algorithms and techniques deployed for testing of human cardiopulmonary characteristics.

3.6.1 Center Estimation Algorithm:

In practical Doppler radar testing, the acquired baseband signal is subject to dc offset due to homodyne mixing with non-modulated RF components reflected from stationary clutter. This causes the arc traced by the in-phase and quadrature channels to be offset from the origin of the plot. The role of the center estimation algorithm is to locate the circle to which the arc belongs and bring the center of the circle to the origin of the complex I-Q plot. The radius of the centered circle is the magnitude A of the baseband signal. It corresponds to the power of the reflected wave which

is proportional to the effective radar cross section. The center estimation algorithm is implemented in three steps [68] [69] demonstrated in Fig. 3.6. First, the algorithm finds the mean of the complex baseband signal and subtracts it from the signal. The mean includes the residual dc offset and almost the entire radius. This brings the arc to the origin of the coordinates. Second, the arc is rotated to be parallel to the y-axis using the matrix of eigenvectors of the covariance matrix [69]. Hence, the center of the circle will be located on the x-axis. Last, the center is obtained knowing that the bisector of the line joining any two points on the arc passes through the center of the circle. Since the signal is noisy by nature, a bisector is obtained for every two successive points on the arc and a statistical median is applied on the resulting centers. Once the center is known, the circle is centered at the origin and the radius A is obtained by taking the root mean of $(I_{BB}^2 + Q_{BB}^2)$.

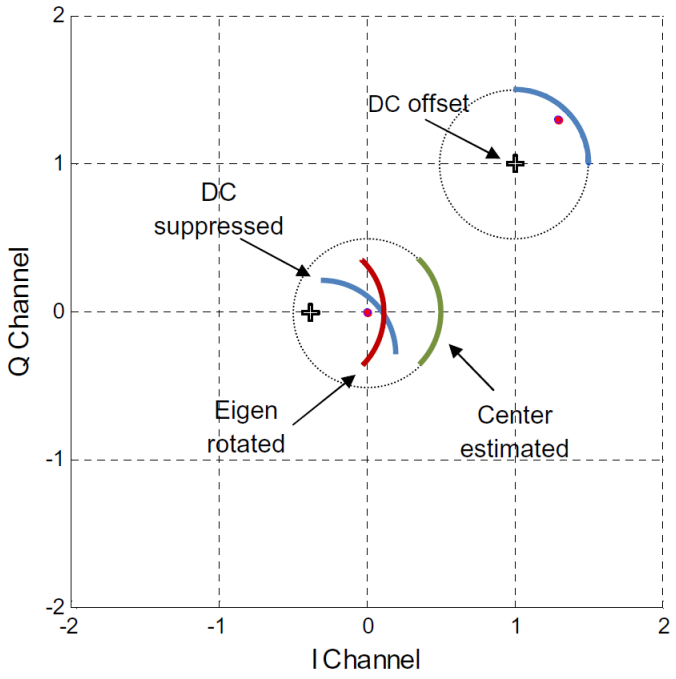

Fig 3.9: Demonstration of central estimation Algorithm in steps

3.6.2: Closed Loop DC Cancelation System:

The dc content of the baseband signal combines the radius A and the dc offset due to stationary clutter. Since the signal received from the moving target has a power that is proportional to A_2, it is necessary to recover the value of A to determine the effective radar cross section. In principle, the center estimation algorithm does not require cancellation of the dc offset in the baseband signal. However, due to the potentially high dc levels and due to the limited number of bits in the data acquisition system, it is required to minimize the dc offset to maximize the accuracy by which the ac signals are acquired [70] [71] and to allow cancellation of random body motion

[72]. The dc-cancellation approach used allows coupling the baseband signal to the low noise amplifier while preserving the low frequency content. It represents an alternative to ac coupling which results in distortion of the low frequency components making it difficult to accurately recover the radius A [73].

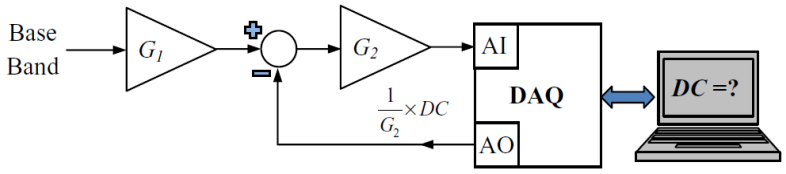

Fig 3.10: Schematic block diagram of the dc cancelation system

In the setup deployed, the dc offset is minimized using a technique like that of Vergara et al. [74]. The dc value is estimated from the measured signal itself and is fed back, with negative polarity and correct scaling, to the baseband signal just before the last filtering and amplification stage. The operation of the dc cancelation system is demonstrated in Fig. 3.13. The baseband signal is amplified on two stages. With the output being digitally acquired, the signal processing station calculates the mean, divides its value by the second amplifier gain and sends it to the analog output port of the data acquisition device. The second amplifier then amplifies the difference which ideally has suppressed dc content. This process is continuously looping during measurements to maintain the dc offset of the acquired signal within the desired limit.

3.6.3 ERCS Measurement:

The radar cross section represents the amount of the power density that is reflected off a target with respect to the power incident on the target. In human cardiopulmonary testing, the target is the surface of the torso moving due to respiration and heartbeat and results in an effective radar cross section (ERCS). The complex baseband signal detected at the receiver traces an arc on the I-Q plot such that the radius of the arc equals to the amplitude A of the time varying signal. While the arc radius A is calculated by the center estimation algorithm, the dc offset caused by the signal returning from stationary objects is inherently rejected by the algorithm as shown in Fig. 3.6. Knowing the transmitted signal power and the different losses in the system, the relation between the ERCS and A^2 can be calculated.

The calculation of the amplitude A requires having both the in-phase and quadrature components of the baseband signal. Due to the nature of the time varying signal, the relation between A and the average power of the individual I or Q depends on the total phase $\Omega(t)$ in the argument of the cosine and sine functions in (3.16) and (3.17). The value of the total phase depends

on the motion amplitude of the target, reflection phase ϕ_o and target range. The motion amplitude determines the magnitude of the time varying phase while the reflection and range contribute to the constant phase offset ϕ_{tot}.

The effect of the target characteristics on the single channel power is illustrated using the example of Section 3.1.2 for a 2.4 GHz system. The baseband equations are:

$$I_{BB} = A\cos(x(t) + \phi_{tot}) \tag{3.19}$$

$$Q_{BB} = A\sin(x(t) + \phi_{tot}) \tag{3.20}$$

Since the target characteristics are unknown, the amplitude A cannot be estimated by obtaining the root-mean square of the single channel. But it is possible to calculate A by having the root-mean square of both channels because for all values of ϕ_{tot}, the ratios of root mean square voltage, V_{rms} to A of the I-channel and Q-channel satisfy the following:

$$\frac{(V_{rms})_I^2}{A^2} + \frac{(V_{rms})_Q^2}{A^2} = 1 \tag{3.21}$$

Therefore, a quadrature receiver is required to obtain the in-phase and quadrature channels to calculate the amplitude of the complex baseband signal and the effective radar cross section. In addition, the root-mean square of each channel cannot be obtained by directly measuring the average power of the RF signal in the receiver or by processing the baseband signals individually. Although the phase-modulated RF is a narrow-band sinusoid with a known relation between A and average power, this signal is associated with the single tone sinusoid due to reflection from clutter and stationary parts of the body. The power of each component is not separable in the RF band and only signals from moving parts are of interest to measure the effective radar cross section resulting from the human cardiopulmonary activity. At the output of the mixer, the dc content in the baseband due to stationary objects is not separable from the dc information associated with the signal. Therefore, both baseband channels must be combined to obtain the arc they trace on the complex I-Q plot. The radius of the arc can then be obtained using the center estimation algorithm which is independent of the dc content in the signal.

3.6.4 Torso Displacement Movement:

On the complex I-Q plot, the arc traced by the baseband signal scans an angle that corresponds to the time-varying phase in the argument of both the cosine and sine. The center estimation algorithm locates the circle to which the arc belongs and places its center at the origin. By applying arctangent to the start and end points of the arc, the corresponding angles are calculated. The difference between the two angles is the angle $\Delta\Omega$ scanned by the arc due to the

displacement of the target. The value of the displacement, Δx, is calculated from the argument of the cosine function in (3.17) as follows:

$$\Delta x = \frac{\lambda}{4\pi}\Delta\Omega \tag{3.22}$$

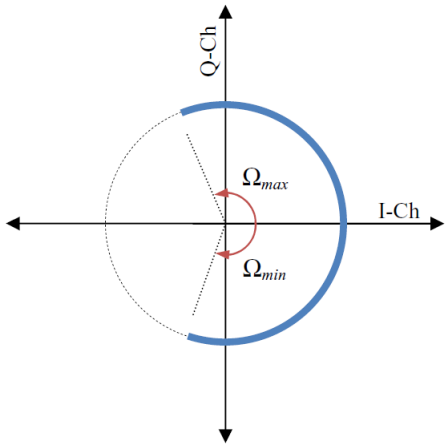

Fig 3.11: Scanned angle Estimation [75]

In order to locate start and the stop points of the arc, the algorithm deployed rotates the arc such that it is parallel to the y-axis, as shown in Fig. 3.15. The arctangent is then applied to all points on the arc and the resulting values are "unwrapped". The difference between the maximum angle Ω_{max} and minimum angle Ω_{min} is the total angle $\Delta\Omega$ scanned by the arc.

3.6.5 Heartbeat and Respiration Rate Measurements:

In human testing with Doppler radar, the time varying phase of the reflected wave is proportional to the displacement of the torso including heartbeat and respiration. By having the baseband signal in quadrature form, the total angle can be extracted using arctangent demodulation [73] as follows:

$$\tan^{-1}\frac{Q_{BB}}{I_{BB}} = \tan^{-1}\frac{\sin(\Omega(t))}{\cos(\Omega(t))} = \Omega(t) \tag{3.23}$$

where the in-phase and quadrature components are those of the arc relocated with center estimation algorithm. Since the heartbeat amplitude is small compared to that of respiration, the time varying phase $\Omega(t)$ is synchronous with the respiration waveform. Therefore, the respiration rate equals the number of waveform cycles divided by the time elapsed.

To obtain the heart rate, the signal must go through a band pass digital filter with 3-dB cutoff frequencies of 0.88 and 2.92 Hz. The lower and upper cut-offs are selected for average heart rate of humans [75]. The filtered signal is then divided into 8-sec segments that are auto-correlated [76] and the resulting rates from all segments are averaged. When the angle scanned by the arc is relatively small, Eigen-function processing is a good alternative to arctangent demodulation. It consists of rotating the arc such that it is parallel to the y-axis. The respiration and heartbeat rates are then extracted from the imaginary part only. This algorithm does not require accurate estimation of the arc radius and it is basically equivalent to single channel receiver at optimum point. In the setup deployed for human testing, the respiration cycles are detected by counting the number of zero-crossings of the raw baseband signal that is not at null point or the reference signal from the effort belts.

3.7 System Design Trade-off:

The Doppler radar system consists of physical and digital layers. The former includes the RF domain where the Doppler effect occurs and also includes the baseband and signal acquisition parts. The digital layer is represented by the digital signal processing that is applied both real-time and post measurement. In each layer, the design parameters determine the overall performance of the system depending on the target application. This section presents the major tradeoffs in the implementation of Doppler radar systems for human testing.

3.7.1 AC-DC Coupling Tradeoff:

The dc content in the baseband signal is partially due to the demodulated single tone carrier reflected from stationary clutter. Other, dc information is inherent to the signal. In general, the overall dc level in the received signal can be high in relation to the time varying content. During signal acquisition, the limited number of bits in the analog to digital converter requires that the dc content of the signal be removed to accurately detect the time varying information.

The dc-cancelation circuit explained in Section 3.6.2 demands additional signal processing in real-time during acquisition. In addition, if the subject changes his/her position or rolls in bed such that the actual range is modified, the new dc value must be calculated and fed to the negative input of the LNA. This introduces some settling time of a few seconds till the acquired dc level reaches the desired level. An alternative would be to use ac coupling at the input of the low noise amplifier. However, the roll-off of the ac coupling filter causes distortion to the lower frequency components of the signal.

In respiration signal the slow-motion characteristics can be accurately captured with dc coupling, tilts are introduced in the ac coupled signal due to distortion to the actual respiration motion. However, the respiration rate is similar in both coupling techniques. Therefore, ac coupling is optimum if rate measurements are the sole application of the system. But for radar cross section measurement, the dc information must be maintained through dc coupling and dc cancelation must be applied.

3.7.2 Eigen-Arctangent Demodulation Tradeoff:

With the baseband signal being in form of two quadrature components, an accurate estimate of the time varying phase is possible with arctangent demodulation. This algorithm requires locating the circle of the arc defined by the I-Q channels and bringing it to the origin of the plot. Hence, it must be associated with the center estimation or circle fitting algorithm. The resulting phase is proportional to the motion of the human torso, including the heartbeat and respiration. This signal is further processed to extract the heart and respiration rates. In addition, the maximum scanned angle is proportional to maximum torso displacement and, when the subject is facing the transceiver, it is an indication of the respiration depth of the subject. The radius of the center estimated arc is used for measuring the effective radar cross section.

For rate measurements only, Eigen function demodulation represents an alternative to arctangent demodulation. This algorithm is equivalent to a single channel receiver where the baseband signal is at optimum point. It consists of rotating the vector of complex data such that the arc traced by the in-phase and quadrature channels is parallel to the *y*-axis. Therefore, the projection of the arc on the y-axis is proportional to the time varying phase and is used to obtain the heart and respiration rates. Since the variation along the *x*-axis is neglected, a better accuracy is obtained when the angle scanned by the arc is small, less than 60°, so that the arc is approximately a straight line. This condition depends on the operating frequency as well as the maximum torso displacement during respiration. The center estimation of the arc becomes unnecessary, but the displacement and RCS measurements become invalid.

3.7.3 Operating Wavelength Tradeoff:

In the physical layer of a Doppler system, a major design parameter is the operating radio frequency. This is the frequency at which the carrier is transmitted and at which all the RF devices are tuned. It also affects the RCS value of the target as well as the amount of phase deviation due to the target displacement. First, the selected wavelength λ must satisfy all conditions of far-field measurements for a given target range. For resonant antennas, the size of the radiator is in order of $\lambda/2$. The radiation far-field condition requires small wavelengths such that the target range is much larger than λ. On the other hand, for a fixed target size d, the plane-wave incidence condition requires larger wavelength so that the target range is larger than $2d_2/\lambda$.

For the average size of a human adult and for operating frequencies at 2.4 GHz and beyond, the plane-wave condition is dominant. This implies that smaller wavelengths demand larger target ranges to maintain far-field measurements. In addition, since Doppler analyses assume small target displacements with respect to the range, the assumption is more accurate at larger ranges where the amplitude distortion due to the target motion can be neglected. However, large target ranges cause a reduction in the signal to noise ratio. From Friis transmission formula and for a fixed generator power:

$$P_R \propto P_T \frac{\lambda^2}{R^4} \tag{3.24}$$

Therefore, higher generator power is required to maintain the same received signal power at a larger distance. Second, in terms of system resolution, the amount of phase deviation due to torso displacement is inversely proportional to wavelength:

$$\Delta\Omega = \frac{4\pi}{\lambda}\Delta x \tag{3.25}$$

On the complex I-Q plot, the phase deviation is the angle scanned by the arc traced by the baseband signal. Therefore, detecting small motion requires larger operating frequencies. From the far-field conditions, increasing the frequency demands large target ranges which affect the signal to noise ratio.

Last, from Mie relation of radar cross section, the value of the RCS of a spherical target is a function of the operating wavelength. If the frequency of operation is such that the target size falls in the resonance region, the RCS presented by the target is not monotonically increasing with the target size. In order to compare two unknown targets using RCS measurements, the operating wavelength must be small with respect to the circumference of the physical cross section of the targets. This allows optical region analyses where the relation between targets of different sizes or different shapes is well defined. For the average human torso, the chest breadth $2a$ is about 30 cm. To have $2\pi a/\lambda$ greater than 10, frequencies above 3 GHz are desired.

3.8 Physiological Radar Monitoring System (PRMS) Architecture:

A non-contact physiological radar monitoring system (PRMS) is introduced by Mehran Baboli [Baboli] for sleep disorder monitoring. This PRMS utilizes continuous-wave Doppler radar and a real-time algorithm which recognizes paradoxical breathing to diagnose OSA and hypopnea. The PRMS was integrated with a standard PSG system to evaluate the efficacy for supplementing or replacing a standard PSG test for some applications.

The current gold standard and arguably best way to study sleep apnea is Polysomnography (PSG). Polysomnography makes comprehensive recordings of the biophysiological changes that happen during sleep. The PSG monitors many body functions during sleep such as: brain activity (EEG),

eye movements (EOG), muscle activity (EMG), heart rhythm (ECG), respiratory airflow and respiratory effort. Several systems available in the market for sleep studies such as SomnoStar® z4 Sleep System, from CareFusion (http://www.carefusion.com), Sapphire PSG™ with its complementary software Cyrstal PSG™ Software from Cleveland Medical Devices Inc, [78] and Sandman Elite PSG Software with its complementary hardware from Embla [77]. In the project, all the tests were carried out in Queens Medical Center [79] which uses Sandman for sleep studies. Hence, it was considered as a gold standard for the project [28].

The planned overnight sleep study will take place in a certified sleep study center at Queen's Medical Center in Honolulu, Hawaii. The size of the room will be approximately 5×6 m^2. Because the PRMS must be placed in the room without obstructing the normal movements of the subject, it should compact. Careful placement of the radar is also critical as Doppler radar is most sensitive for motion that is orthogonal to the plane of its antenna.

The PRMS architecture was developed with one receiver to cover both chest and abdominal movement. The second receiver was kept as a backup to insure recording high quality signals in case. Furthermore, the sensitivity of the Doppler radar to the motion sensitivity changes with the frequency of its operation. The PRMS have two quadrature Doppler radar systems transmitting at 2.4 GHz and 24 GHz integrated into a package 20cm×15cm×8cm in size.

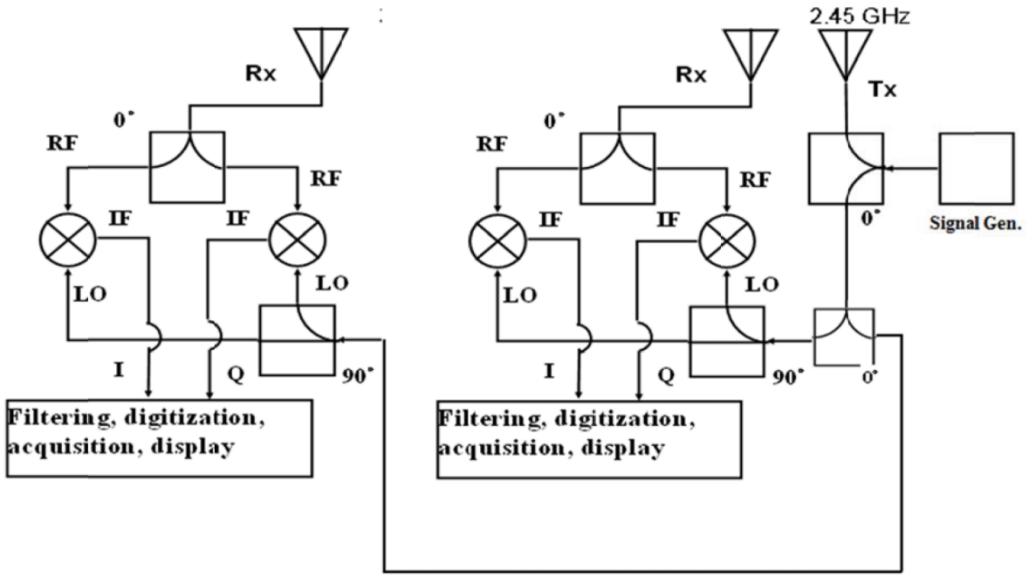

Fig 3.12: Doppler radar architecture for PRMS system with common transmitter and two receivers to track physiological motion [28]

In [28], coaxial components were used to implement the Doppler radar with 2.45GHz. An oscillator with fixed power was used to generate the signal at 2.45GHz and the transmitter power was varied using a step attenuator [80] placed in the 2.4 GHz transmitter path. The ZFSC- 2-2500 splitter [81] divides the source signal into the transmitter antenna and local oscillator paths with 90o phase difference. Three ASPPT2988 panel antennas [82] was configured as one common transmitter and two receivers. The antenna pattern is shown in Figure 3-10. ZFM-4212 frequency mixer [83] was used to extract the baseband signal from RF input. Then the signal was fed to the differential input of the SR560 [84] low noise amplifier for DC cancellation, amplification and filtration.

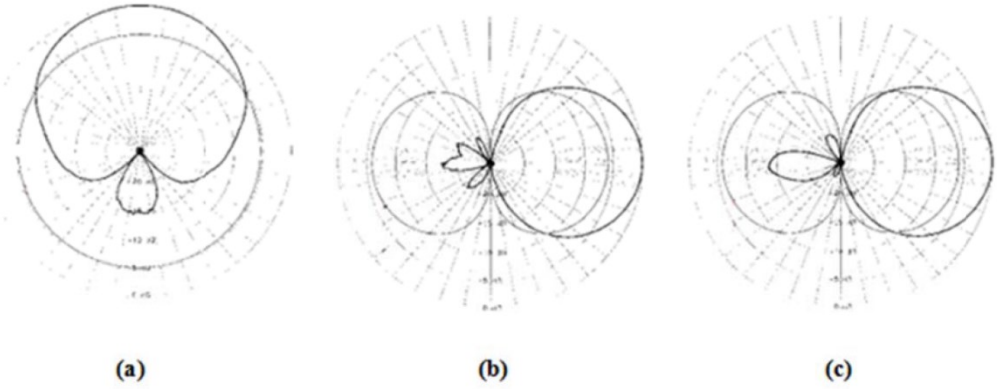

Fig 3.13: 2.4 GHz antenna pattern (a) H-plane (80 deg) Dipole Reference (b) E-plane (60deg) Dipole reference and (c) E-plane (65 deg) Dipole reference [82]

The 24 GHz radar was a commercial off the shelf 24 GHz module K-MC1 from RF beam [85]. This module has 24GHz K-band antenna with I/Q Mixer and IF-Preamplifiers. The antenna pattern is shown in Figure 3-13. The outputs of 24GHz were also fed into SR560 low noise amplifier. Both radar outputs were amplified with the gain of 200 and filtered with a low pass frequency with the cut-off frequency at 30Hz.

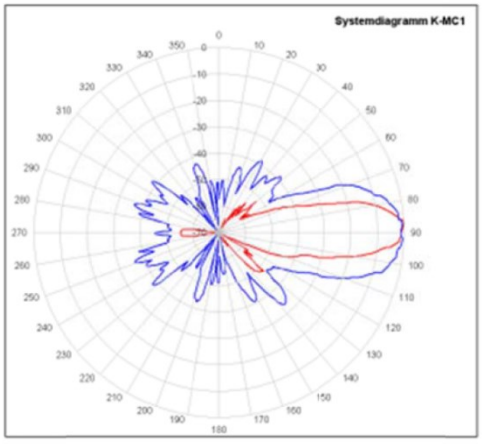

Fig 3.14: 24 GHz antenna pattern [85]

Finally, all baseband output are converted from analog to digital using National instrument data acquisition module (NI-USB 6259 [86] and sent to MATLAB to be analyzed using sleep monitoring algorithm. The same DAQ was used to send the outputs to Sandman in [28] their work. Figure 3.12 show the input/output ports arrangement and Figure 3.13 show the antenna board setup they used in their experiment [28].

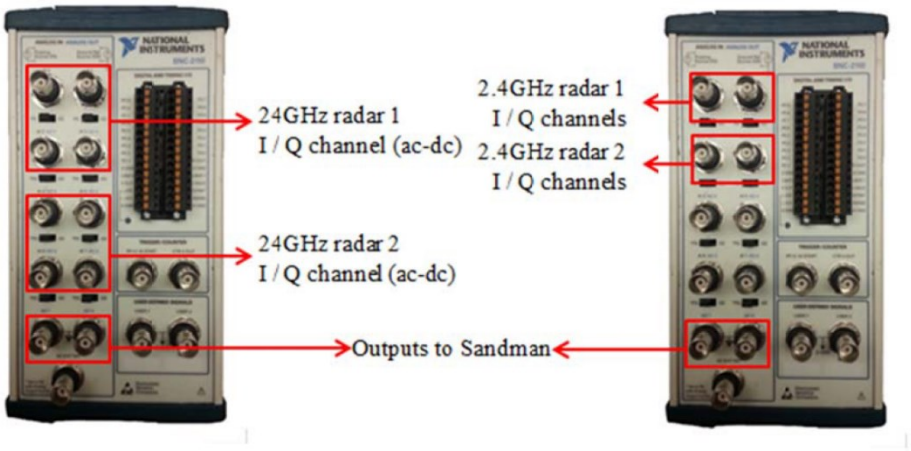

Fig 3.15: Analog inputs/outputs arrangement [28]

Fig 3.16: Antenna board panel [28]

Chapter - 4

Radar Cross Section

In radar measurements of an unknown object, a major parameter for target recognition is the effective cross section that the object represents to the illuminating wave. It is proportional to the magnitude of the reflected wave detected at the receiver, and with system calibration its actual value can be calculated. This chapter presents the definition of the radar cross section of a target and demonstrates the analytic solution for basic geometrical shapes to understand its characteristics. The measurements of arbitrary targets with Doppler radar are then explained as well as the conditions required to perform accurate identification of the radar cross section.

4.1 Radar cross section:

The radar cross section (RCS) is a measure of the magnitude of the wave echoing back from the target and hence it is an indication of how detectable an object is with radar. The value of the radar cross section, s, is such that the power scattered off the target results from the product of the incident power density with the radar cross section:

$$P_s = S_i \cdot \sigma \tag{4.1}$$

where *Ps* is the power scattered and *Si* is the incident power density at the target. When the wave is scattered equally in all directions, the power density at the radar receiver *Sr* is equivalent to the scattered power per unit area of a sphere having a radius *R* equal to the target range:

$$S_r = \frac{P_s}{4\pi R^2} \tag{4.2}$$

In terms of incident and reflected electric fields, the radar cross section is expressed as:

$$\sigma = \lim_{R\to\infty} 4\pi R^2 \frac{|E_\pi|^2}{|E_i|^2} \tag{4.3}$$

where *Ei* is the incident electric field at the target and *Er* is the reflected electric field at the radar receiver. The limit of *R* tending to infinity aims to consider far-field targets where the incident radiation is a uniform plane wave, leading to the IEEE definition of radar cross section [70]. Descriptively, the radar cross section of a target is a fictional area that intercepts the incident

wave that, if scattered uniformly, produces an echo power at the receiver equal to that produced by the real target.

In general, the RCS depends on the physical characteristics of the target namely size, shape, and material of its surface. For a defined target, the radar cross section can be calculated by solving Maxwell's equations and applying appropriate boundary conditions. On the other hand, measurements of arbitrary targets are based on the radar equation and proper system calibration.

4.2 RCS of Basic Geometrical Objects:

Analytical solutions for radar cross sections are possible for targets with simple geometrical shapes. This is especially true at high frequencies where specular reflections are assumed. This section presents the solutions for spherical and cylindrical bodies as well as flat surfaces. Results obtained in these cases give an insight into the dependence of radar cross section on target geometry and operating frequency. They also facilitate the understanding of radar cross sections of human subjects.

4.2.1 Three-Dimensional Sphere:

The radar cross section of a perfectly conducting sphere is obtained from Mie series solution of wave scattering [87]. The solution of Mie series is valid for any frequency and sphere size. A plot of this solution versus frequency is shown in Fig. 3.1, like the representation of Skolnik [88]. The RCS is normalized with respect to physical cross section area while the circumference with respect to wavelength.

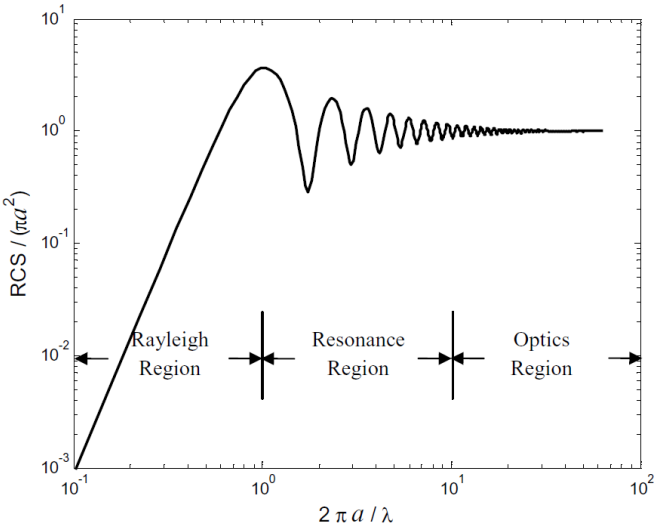

Fig 4.1 Radar Cross-section of metallic sphere of radius,a as function of wavelength [75]

As observed, the variation of the RCS with frequency is classified into three different zones. At relatively low frequencies, the RCS increases with frequency due to Rayleigh scattering. At intermediate frequencies where the wavelength begins to be exceeded by the circumference of the sphere, the RCS is the result of the superposition of specular reflection from the front and a wave creeping on the back and returning to the front, as shown in Fig. 3.2. The creeping wave is due to multiple diffractions on the curved surface of the sphere.

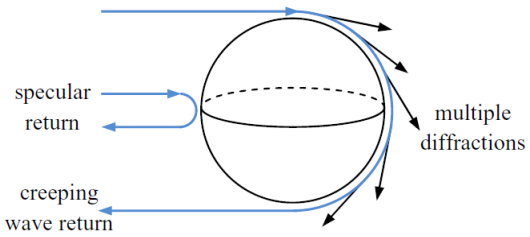

Fig 4.2 Two types of waves scattering off a metallic sphere [75]

The two components may combine in phase or out of phase depending on frequency. This leads to fluctuation of RCS in this zone that is called resonance region. As frequency increases, the magnitude of the creeping wave diminishes, and the specular return becomes dominant. This corresponds to the optical region where the incoming wave illuminates the sphere with a bright spot at the specular point. In this case, the radar cross section of the perfectly conducting sphere becomes equal to the physical cross section area, $\sigma = \pi a^2$.

4.2.2 Cylindrical Body:

For an infinitely long cylinder perpendicular to an incident wave, the radar cross section per unit length depends on the polarization of the wave with respect to the cylinder axis. In the backscattered direction, the Mie series solution for perfectly conducting cylinders [87] is:

$$\sigma_{TM} = \frac{2\lambda}{\pi}\left|\sum_{n=0}^{\alpha} \varepsilon_n(-1)^n \frac{J_n(\beta a)}{H_n^{(2)}(Ba)}\right|^2 \tag{4.4}$$

$$\sigma_{TE} = \frac{2\lambda}{\pi}\left|\sum_{n=0}^{\alpha} \varepsilon_n(-1)^n \frac{J\prime_n(\beta a)}{H_n^{\prime(2)}(Ba)}\right|^2 \tag{4.5}$$

where a is the radius of the cylinder, and σ_{TM} and σ_{TE} respectively correspond to solutions for magnetic and electric fields transverse to the cylinder axis. The coefficients ε_n are integers such that:

$$\varepsilon_n = \begin{cases} 1 & n = 0 \\ 2 & n \neq 0 \end{cases} \tag{4.6}$$

The primes on the Bessel and Hankel functions indicate derivative with respect to the argument. The ordinary Hankel function consists of ordinary Bessel functions $J_n(x)$ and $Y_n(x)$ of first and second kinds, respectively:

$$H_n^{(2)}(x) = J_n(x) - iY_n(x) \tag{4.7}$$

In the optical region, σ_{TM} and σ_{TE} converge to one value and the radar cross section becomes independent of polarization. From the theory of specular scattering [87], the backscatter radar cross section of any object takes the form of:

$$\sigma = 4\pi \frac{(A_{ef})^2}{\lambda^2} \tag{4.8}$$

where A_{eff} is the effective area of incidence from which reflected components add in phase. For curved surfaces, it is considered as the area at the specular point where the phase variation is within $22.5\,\text{deg}$ or $\lambda/16$.

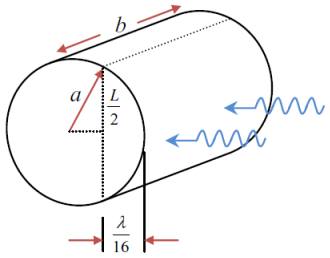

Fig 4.3 Specular effective area of a metallic cylinder

For the finite cylinder in Fig. 4.3, the constant phase region for normal incidence has a length *b* and a width *L* such that:

$$\frac{L}{2} = \sqrt{a^2 - \left(a - \frac{\lambda}{16}\right)^2} \tag{4.9}$$

The condition of specular reflection is satisfied when $2\pi a/\lambda > 10$. Therefore, the radius a is much larger than $\lambda/16$, and the width is approximated to:

$$L \approx \sqrt{\frac{a\lambda}{2}} \tag{4.10}$$

This leads to the solution of radar cross section for a perfectly conducting cylinder in the optical region:

$$\sigma = \frac{2\pi ab^2}{\lambda} \tag{4.11}$$

The same analyses can be applied to obtain the radar cross section of a perfectly conducting sphere in the optical region. In this case, the effective area is equal to L^2 where L is from (4.10).

4.2.3 Rectangular Plate:

The radar cross section of a perfectly conducting plate in the optical region is also derived from the theory of specular reflections. For normal incidence on a flat surface, the reflected components are all in phase and the effective area equals to the physical one. Therefore, the radar cross section is:

$$\sigma = \frac{4\pi . A_{ph}^2}{\lambda^2} \tag{4.12}$$

where A_{ph} is the physical surface area of the rectangular sheet. This relation can be generalized for any flat surface normal to the wave since specular reflections are independent of the plate geometry.

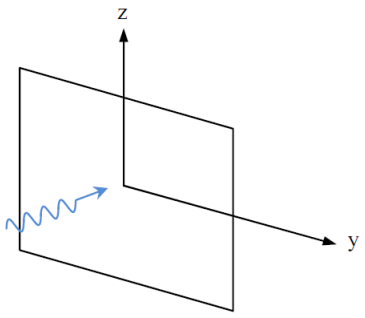

Fig 4.4 Wave incidence of rectangular metallic sheet [75]

The comparison between the solution for a cylinder to that for a flat plate shows that the curvature of the cylindrical surface results in a reduction in its effective area with respect to its projected rectangle. This demonstrates that two surfaces having the same projected cross

section, but different curvatures will show different radar cross sections where the larger belongs to the less curved surface, i.e. larger radius of curvature.

Based on the concept of effective area and from the results of human testing, John Kiriazi in his thesis [75] modeled the human torso as a half-cylinder where the front body corresponds to the curved surface and the back to the flat one. The width of the flat surface is equal to the diameter of the cylinder as shown in Fig. 4.5. For a perfectly conducting body in the optical region, the ratio of the radar cross section of the back to that of the front is calculated using the optical region formulas for a rectangular plate and a cylinder:

$$\frac{\sigma_{back}}{\sigma_{front}} = \frac{4\pi(2ab)^2/\lambda^2}{2\pi ab^2/\lambda^2} = \frac{8a}{\lambda} \tag{4.13}$$

The resulting ratio is a function of wavelength. The Doppler radar developed for human testing uses two frequencies, 2.4 and 5.8 GHz which correspond to wavelengths of 12.5 and 5.17 cm respectively. Considering the average human chest breadth to be 30 cm, the radius of the cylinder is half of this value. This leads to RCS ratios of 9.6 and 23.2 at the lower and higher frequency, respectively.

For the side of the body, a wave that is incident normally on the side of a half-cylinder will see an area of constant phase having a width *b* and a length *L*/2. The ratio of radar cross section of the side with respect to front is calculated as:

$$\frac{\sigma_{side}}{\sigma_{front}} = \frac{\pi ab^2/\lambda}{2\pi ab^2/\lambda} = \frac{1}{4} \tag{4.14}$$

This indicates that the radar cross of the side is expected to be a quarter that of the front independent of frequency.

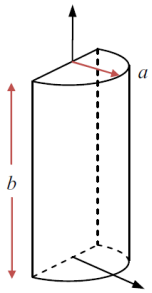

Fig 4.5 A metallic half-cylinder

The relatively large discrepancy between RCS of front and back of the human torso is the key parameter to identify the orientation of the subject with respect to the transceiver. Therefore, in

the Doppler system design it is important to use an operating frequency that allows near optical scattering. On the other hand, the target range must satisfy the conditions of far-field measurements so that the derived RCS equations are valid.

4.3 RCS Measurement of Arbitrary Objects:

From the definition of radar cross section, if the power density incident on a target and the amount of power reflected are known, the RCS can be measured for objects of any shape or material composition. This is allowed through design and characterization of a radar system featuring detection of magnitude of received signals. The relation between the transmitted and received powers is described by the radar equation. However, wave propagation effects impose some challenges to accurate RCS measurements. These include propagation between the transceiver and target as well as in the surrounding environment. A detailed explanation of parameters affecting the radar cross section measurement is presented in Section 4.4. This section discusses the intrinsic propagation characteristics of the wave traveling between the radar and target.

4.3.1 Radar Equation:

The radar equation is based on Friis law applied on two-way propagation. Given the target range, the power density incident on the target is a result of spherical wave radiated from the transmitter antenna and is expressed as:

$$S_i = \frac{P_T G_T}{4\pi R^2} \tag{4.15}$$

where P_T is the power emitted by the antennas, G_T is the antenna gain, and R is the range. The power density at the receiver is due to spherical propagation of the scattered wave off the target and is given in equation (2.2). The actual power detected at the receiver antenna is the received power density collected by the effective area of the antenna:

$$P_R = S_r A_{eff} \tag{4.16}$$

Where P is the received power and A_{eff} is the effective area.

Expanding the latter terms of antenna gain, G_R, and using substitution from (4.2) and (4.1), the radar equation becomes:

$$P_R = P_T \frac{G_T G_R \sigma}{(4\pi)^3} \frac{\lambda^2}{R^4} \tag{4.17}$$

The transmitted and received powers are those at the antenna end. A calibration with a known target is then required to relate these values to actual input and output powers of the radar system. Once the system is characterized, it can be used to measure any other target.

4.3.2 Far field Condition:

As the wave is radiated from the transmitter antenna, it undergoes different phases along the propagation path leading to the target. While the radar equation is valid only for propagating waves, radar cross section theory assumes plane wave incidence. This requires the target to be placed in the far zone of the antenna where propagating waves dominate stationary fields and where spherical waves are effectively planar in relation to the target size [89] [90]. The far-zone distance is a function of the operating frequency and the dimensions of both the target and the antenna.

The magnitude of the backscattered wave from a target depends on the phase of the reflected components. If the incident wave itself has spatial phase variation, the magnitude of the reflected wave will be affected accordingly. This requires that the wave front of the incoming wave be planar to achieve accurate RCS measurements. Wave radiated out of a source is in spherical form. However, if the target is far enough from the source, the incident wave along the cross section of the target is approximately planar. The minimum value of target range to consider the source radiation as a plane wave is when phase variation of the spherical wave along a reference plane with the cross-section of the target does not exceed 22.5 deg or $\lambda/16$.

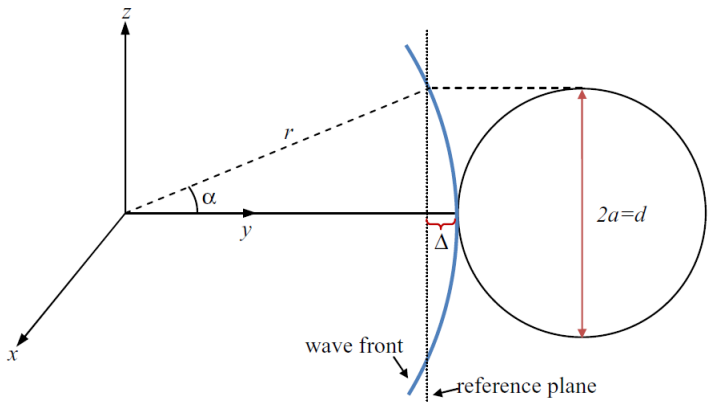

Fig 4.6: Geometry of a scattering problem

For target having a diameter d=2a, the distance of maximum error is derived from the geometry of Fig. 4.6 and is equal to:

$$\Delta = r - r \cdot \cos\left(\tan^{-1}\frac{a}{r}\right) \tag{4.18}$$

If the range is such that r > 8a, the error D can be approximated to $a^2/2r$. Therefore, the wave planarity far-field condition becomes:

$$r \geq \frac{2d^2}{\lambda} \tag{4.19}$$

4.4 Cardiopulmonary Effective RCS measurement:

When the target under test is moving, the returning signal of the CW radar is phase modulated by the Doppler effect. This is the case of a human subject where the surface of the torso is moving due to the cardiopulmonary activity of the subject. At the receiver, homodyne mixing of the returning signal with a non-modulated carrier results in a time varying signal. Reflections from clutter and stationary parts of the body result only in a dc offset that is to be eliminated making no contribution to the measured radar cross-section. Therefore, only the effective radar cross section (ERCS) of the moving surface of the body is being measured.

During respiration, the movement of a human torso consists of two moving objects: the thorax and the abdomen. The body surface has a time-space distribution [91] [92] that is determined by the demand-intake chain effect of the two parts. This characteristic varies between humans and is directly affecting the measurements of the effective radar cross section. By kiriazi, the torso of a human subject is modeled as two cylinders that in general have different sizes. When the body demands air to flow into the lungs, the muscles of the thorax expand to allow inhalation. The air first fills the thorax which inflates with a velocity $\upsilon_T(t)$. The abdomen then starts to expand with a velocity $\upsilon_A(t)$. The thorax and abdomen are usually at different altitudes, especially for female subjects [75]. Since, the abdomen motion is delayed with respect to that of the thorax, the latter starts the exhalation process earlier. The abdomen then follows and moves down to the initial position which can be lower than that of the thorax. With continuous respiration cycles, the overall body surface appears like a short non uniform ripple.

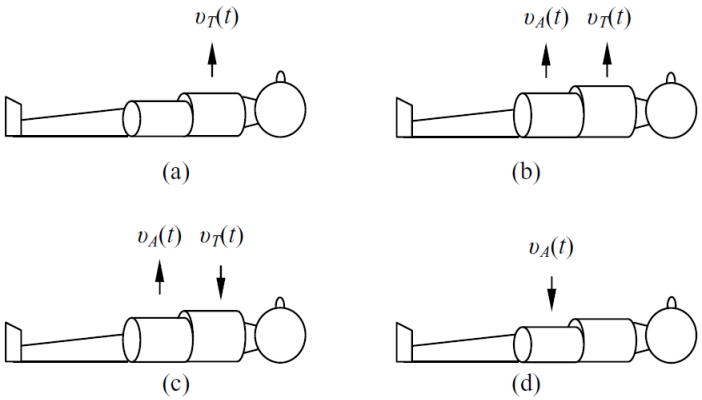

Fig 4.7: Time-space distribution of human torso at (a) start of inhalation, (b) during inhalation, (c) start of exhalation, and (d) end of exhalation [75]

The incident wave of the radar hits the body surface of a human subject including the thorax and abdomen. The body torso represents a reflecting target where more than one object echoes the incident wave [93]. The reflected wave off the moving torso is represented as the superposition of two components that are different in amplitude and that are offset in phase. The amplitude of each component depends on the properties of the thorax and abdomen including size, curvature, and reflectivity. The heart motion in the abdomen is considerably negligible.

4.5 Effective RCS calculation

The radar cross section (RCS) of an object is defined as the ratio between the power reflected by a target and the incident power density. It is essentially a property of the target's reflectivity. it is called electromagnetic signature of the target. The measurement of RCS is profoundly influenced by operating frequency, target orientation relative to radar system, radar waveform, and processing. From the radar equation derived in 4.3.1, the term $\frac{P_T G_T}{(4\pi)(R)^2}$ represents the power density that the radar transmitter produces at the target. Thus, the product $\frac{P_T G_T}{(4\pi)(R)^2}\sigma$ has the dimensions of power (watts), and represents a hypothetical total power intercepted by the radar target.

The equation of RCS, σ from the radar equation is:

$$\sigma = \frac{P_R(4\pi)^3}{P_T G_T G_R}\frac{R^4}{\lambda^2} \tag{4.20}$$

From the signal generator to the radiator the losses are due to the reflection at the 0-degree splitter, the 3-dB splitting factor and the reflection at the transmitter antenna. The additional losses in the Tx path are grouped in two terms, a fixed loss and a variable one. The RF signal is converted to baseband with some attenuation due to the conversion loss of the mixer. It is then fed to the LNA where it is amplified with low noise amplifier, G_{LNA}.

The gain factor includes all fixed losses in the system. The electromagnetic wave encounters several types of losses as it travels through the Doppler radar system to the target and back to the receiver. Some losses are inherent to the system hardware and mainly depend on the operating frequency and the power levels at some stages along the wave path. Other losses are due to the propagation of the wave in space on its way from the transmitting antenna to the target and back to the receiving antenna. While the contribution of the path loss for a given range can be calculated from Friis relation, the loss from the several hardware parts can be estimated from the manufacturer data sheet and by tracking the wave path through the system. To obtain the roundtrip gain factor inherent to the system, the constant gain value is expressed in terms of the measurement parameters. This relation can then be used for system calibration and it is as follows:

$$\Re = \frac{R^4}{\sigma_{Cal}} \cdot \frac{1}{P_{in}} \left(\frac{A}{G_{LNA}} \right)^2 \tag{4.21}$$

where Pin is the input power from the generator, G_{LNA} is the gain of low noise amplifier, R is the range and σ_{Cal} is the radar cross section of the moving target, the amplitude of the baseband signal.

4.6 System Calibration:

The gain factor estimation can also be done in the same system using calibration. A system calibration is possible using an object with a pre-known radar cross section being used as the target. It is more accurate method to establish the absolute RCS level where a standard target is substituted for the target being measured. This method is widely used in static measurements and highly recommended for dynamic measurements if possible. The most common calibration target is the conducting sphere for the following reasons [94]:

1. Its RCS level is well established and can be calculated by well-known techniques
2. It does not require angular alignment
3. Its bistatic response is almost Isotropic, except in the forward scattering region (180° bistatic angle), and provides sensitivity to multipath errors over a wide angular volume
4. Its RCS level is relatively low, which increases the sensitivity to background RCS errors [94].

In this experiment, a spherical metallic mechanical sphere is used as standard target. It is a metallic sphere with diameter d= 15.2 cm. To measure the radar cross section in the backscatter direction, the target is placed at a distance along the line-of-site of the transmitting antenna and in the direction of the main radiation lobe. The actual radar cross section of the spherical targets is calculated from Mie series solution for perfectly conducting spheres [87]. This relation is a function of the sphere diameter and the operating frequency. It is also valid in all regions of operation, whether it is the Rayleigh, resonance, or optical region. In principle, the type of electromagnetic scattering is not critical for calibration purposes since the radar cross section is calculated from the theoretical relation. However, the optical region is preferred to compare targets of unknown sizes by measuring their radar cross section.

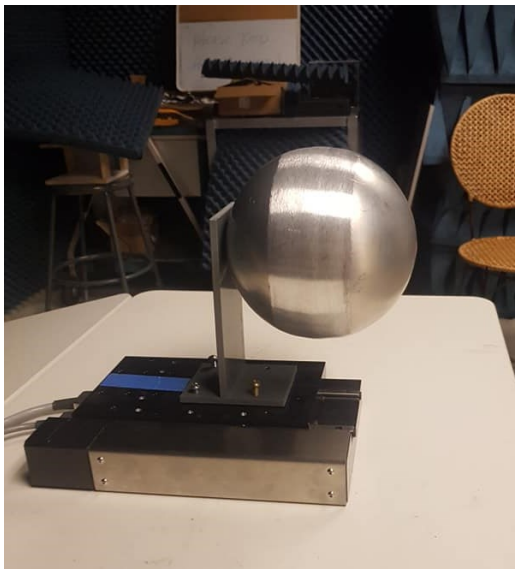

Fig 4.8: Mechanical mover used for system calibration

Since the Doppler radar system detects only moving objects, the target is put into motion via a standard linear mover. This is an automated mechanical device with a stage moving linearly along a single axis. The mechanical mover is aligned such that the direction of motion is in-line with the line-of-sight of the antenna. The mover is programmed to a periodic linear motion with a frequency of 0.2 Hz and amplitudes of 4 cm. These settings are chosen to emulate the practical case of a human subject's respiration. Once the system is calibrated, this constant is used to calculate the effective radar cross section from the measurement parameters by rearranging the loss budget equations in the following form:

$$\sigma_{e_{ff}} = \frac{R^4}{\Re} \cdot \frac{IL_{add}}{p_{in}} \left(\frac{A}{G_{LNA}}\right)^2 \tag{4.22}$$

IL_{add} represents any additional loss inserted in the transmitter path or additional conversion loss and that was not present in the calibrated system, and A is the amplitude of the baseband signal.

Quadrature radio transceiver are subject to amplitude and phase imbalance problems due to hardware imperfections. Theses imbalance corrupt the signal quality and need to be extracted to get actual amplitude A, to calculate corrected RCS. Accuracy of RCS is dependent upon on correction of imbalance and emphasis is on correcting the shape of I-Q arc to obtain corrected value of A. These phase and amplitude imbalance compensation has been done using a mechanical mover and an-ellipse fit method [95].

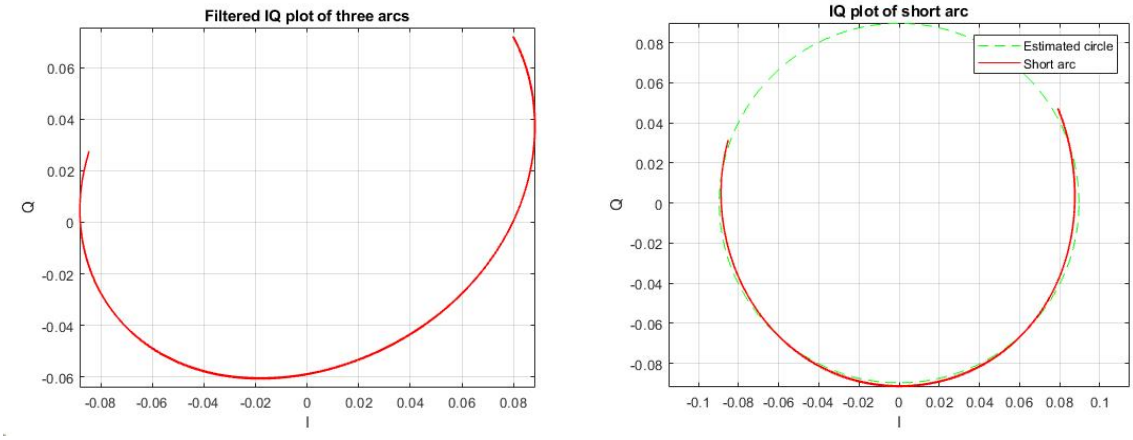

(a) (b)

Fig 4.9: Plot of (a) I/Q data with phase & amplitude imbalance (b) Plot of I/Q data with imbalance compensation

Once the imbalances are known and the radar output can be recovered accurately, measurements must be done with a moving target that has a known RCS. The radar cross section is directly related to the radius estimated and can be calculated by first finding the constant gain value with the known target. To calculate the effective RCS of human subjects, ILadd was set to 1, Pin set to 10dBm, and *A* is replaced with the radius estimated by the circle fitting algorithm for each test.

Chapter - 5

Obstructive Sleep Apnea (OSA) Events Classification

Obstructive Sleep Apnea (OSA) is a sleeping disorder which causes breathing difficulty during sleep. Polysomnography (PSG) is considered as gold standard for sleep apnea diagnosis which is carried out overnight in a specialized hospital-based sleep laboratory [3] with dedicated contact sensors and need a sleep technician. It is uncomfortable, expensive and the medical facilities have a small number of sleep technicians, leading to long waiting lists [4]. In PRMS following AASM manual, it is recommended to use an oronasal thermal sensor to detect absence of airflow for apnea detection. For hypopnea detection, the sensor is a nasal air pressure transducer with or without square root transformation of the signal. All these are contact sensors and painful.

5.1 OSA Events:

OSA is caused by a physical blockage of the airway; it results from airflow obstruction secondary to upper airway collapse or anatomic airway obstruction, even though the respiratory effort is still present. It is characterized by the partial or total collapse of the pharyngeal airway during sleep and the need to arouse to resume ventilation. There are basically two types of obstructive breathing events: Apnea and hypopnea. A common measurement of sleep apnea is the apnea-hypopnea index (AHI). This is an average that represents the combined number of apneas and hypopneas that occur per hour of sleep.

5.1.1 Apnea:

The Greek word apnea means breathless or loss of breath. As defined in American Academy of Sleep Medicine (AASM), apnea presents a 90% or more reduction in airflow compared to the normal baseline [1]. A respiratory event is scored as an apnea when the following criteria are met:

1. Drop in the peak thermal sensor excursion by ≥90% of baseline
2. The duration of the event lasts at least 10 seconds
3. At least 90% of the event's duration meets the amplitude reduction criteria for apnea [96]

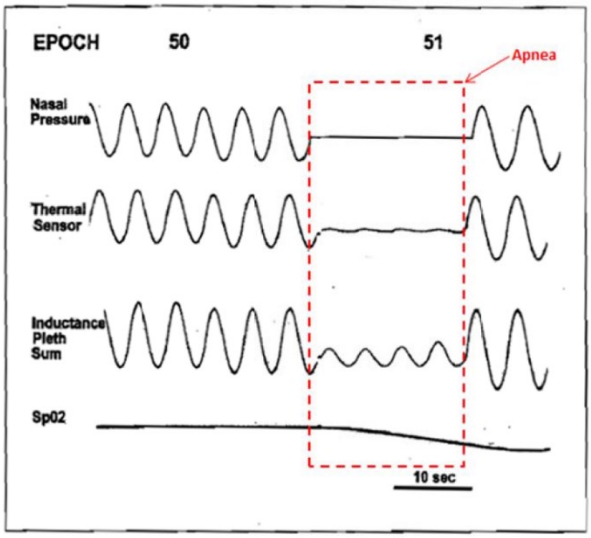

Fig 5.1: Apnea rules [82]

5.1.2 Hypopnea:

Hypopnea presents a 70% or more reduction accompanied by more than 3% oxygen desaturation or arousal [2]. OSA is linked with cardiovascular disease like coronary heart disease, heart failure, atrial fibrillation, morbidity of hypertension and arrhythmia [1]. The recommended criteria for detecting a hypopnea are [96]:

1. Drop of the nasal pressure signal excursions by more than 30% of baseline
2. The nasal pressure drop lasts at least 10 seconds
3. More than 4% desaturation occurs from pre-event baseline
4. Amplitude reduction of criteria for hypopnea happens in at least 90% of the event's duration

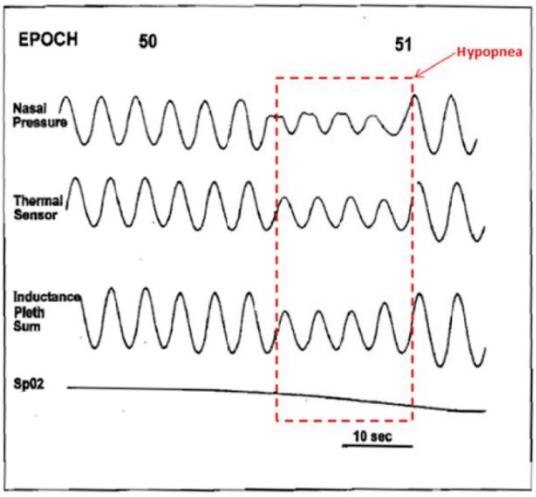

Fig 5.2: Hypopnea rules [96]

5.2 Feature Extraction Algorithm:

OSA events like apnea are hypopnea are identified on basis of several parameters which needs lot of sensors and recorded data using the gold standard PSG system. Recently, smartphone is used to identify apnea event from acoustic sound during breathing but failed to identify many hypopnea events accompanied with snoring properly [97]. Other contactless technology is using infrared cameras but its computationally difficult, privacy concern and efficiency decreases during apnea event compared to normal breathing and movement [27]. Prior research also demonstrated the feasibility of utilizing Doppler radar system to identify different apnea events in comparison to PSG system [4]. However, that proposed system was not automatic as the system utilizes the amplitude-based technique to find different apnea events which requires extensive analysis [4]. In addition to that, ERCS has been utilized to recognize different sleep positions (supine, prone and side) [5]. It has been proved in various investigations that subject sleep positions play an important role in sleep quality and avoidance of certain sleeping position like supine may lead to decrease in the number and severity of obstructive episodes [6].

A uniform, effective and automatic method is required which can determine sleep positions and sleep apnea events also to make the system robust. The feasibility of ERCS method for recognizing different OSA events (normal, apnea and hypopnea) from the clinical study with five different participants utilizing microwave Doppler radar system is investigated. For OSA event classification, two features are extracted from the radar output named:

1) Breathing rate
2) Square of radius of arc

5.2.1. Breathing rate

The respiratory rate in humans is measured by counting the number of breaths for one minute through counting how many times the chest rises. The respiratory rate is the rate at which breathing occurs. The normal respiratory rate for adults is 12 to 18 breaths per minute. The normal respiratory rate for children varies by age. The table below shows normal breathing rate range with age [98]:

TABLE I
RESPIRATION RATE RANGE AS PER AGE

Age	Normal Breathing Rate
Birth and 6 weeks	30-40 breaths per minute
6 months	25-40 breaths per minute
3 years	20-30 breaths per minute
6 years	18-25 breaths per minute
10 years	17-23 breaths per minute
Adults	12-18 breaths per minute
65 years and above	12-28 breaths per minute

Respiratory rate (RR) of a sleep breathing sound signal is an important human vital sign for OSA monitoring during whole-night sleeping. The apnea sections can be detected by the sleep RR values with a given threshold, and the time duration of the segmentation of the breath can be calculated for detailed evaluation of the state of OSA. The RR will be abnormal for the OSA case while the sleep breathing becomes slowed or stopped by the apnea.

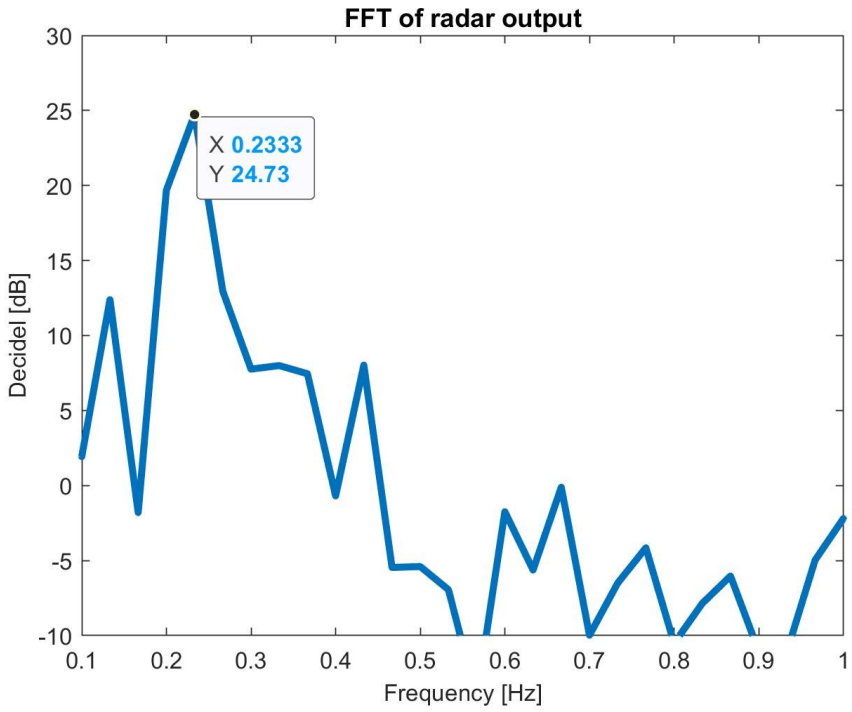

Fig 5.3: FFT of Radar output to get breathing rate

Doppler radar life sign sensing relies on the detection of chest wall motions associated with cardiopulmonary activities. By gathering the Doppler shift content in backscattered signal from the air-skin interface, the variations of the chest wall location as regard to radar can be discerned. It provides safe, clean, non-invasive, and non-contact medical-grade measurement for respiratory rate readings. On basis of process explained in section 3.6.5 using Fast Fourier transformation (FFT) from radar output I-Q data, respiration rate can be measured. In definite time segment from sleep study for OSA patients, the breathing rates for normal, apnea and hypopnea events are noted. The unwanted body movement is separated from radar output as these are several magnitudes larger than chest movement data. The categorized I/Q data is then imbalance compensated. The breathing rate of different OSA events from radar output data are calculated using Fast Fourier algorithm. This is one of the important features for OSA events classification.

5.2.2. Radius of Arc

The measure of the power of the wave bouncing off a radar target with respect to the incident one is defined as the radar cross section (RCS). In human cardiopulmonary testing, the target is the surface of the torso moving due to respiration and heartbeat and results in an effective radar cross section (ERCS) [5]. OSA is associated with airway collapse due to throat muscle relaxation during sleep. The movement of the human torso during respiration varies from person to person and with depth. When there is an obstruction in the airway, paradoxical breathing occurs, and different parts of the torso move out of phase. ERCS correlates with the amount of air flowing into the body during inhalation, namely the tidal volume of respiration. During OSA, power from moving surface of torso changes for change in tidal volume which is reflected in ERCS. During normal breathing, apnea, and hypopnea, ERCS will be different due to different movement contributions from abdomen and thorax. The equation to calculate effective radar cross section, σ from all radar measurement parameter is:

$$\sigma_{e_{ff}} = \frac{R^4}{\Re} \cdot \frac{IL_{add}}{p_{in}} \left(\frac{A}{G_{LNA}}\right)^2 \tag{5.1}$$

It is evident from (5.1) that, for a certain setup ERCS is directly proportional to square of radius of arc, A where all other parameters are constant in that setup. That's why variation of square of radius of arc, A is considered here as a feature to classify OSA events. For second feature extraction, center estimation algorithm on radar output data is used to get radius of Arc, A corresponding to apnea, normal and hypopnea events. In practical Doppler radar testing, the acquired baseband signal is subject to dc offset due to reflection from stationary clutter. This causes the arc traced by the in-phase and quadrature channels to be offset from the origin of the plot [7]. The role of the center estimation algorithm is to locate the circle to which the arc belongs and bring the center of the circle to the origin of the complex I-Q plot.

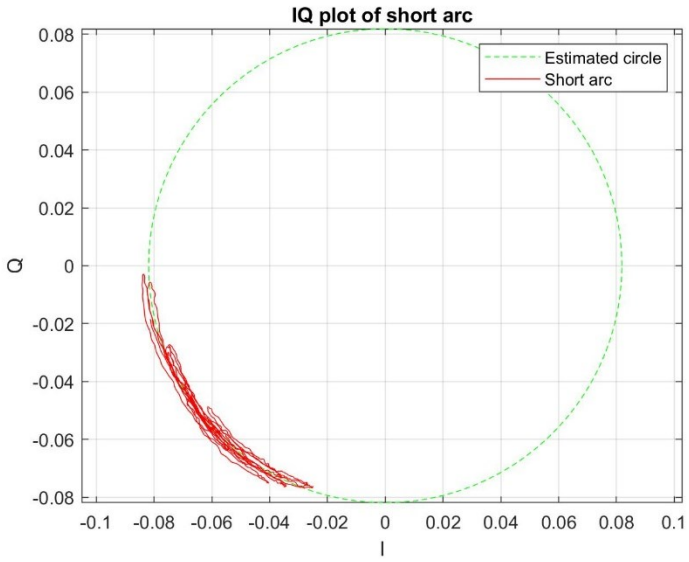

Fig 5.4: Radius of arc implementing center estimation algorithm on radar output data

5.3 Machine learning Classifier:

Machine learning algorithms use computational methods to “learn” information directly from data without relying on a predetermined equation as a model. The algorithms adaptively improve their performance as the number of samples available for learning increases. Two different machine learning classifiers (KNN, SVM) to recognize different OSA events from ERCS and breathing rate measurement of the participants from different episodes of the clinical study are integrated. The two classifiers are:

1. KNN (k-nearest neighbor)
2. SVM (support vector machine)

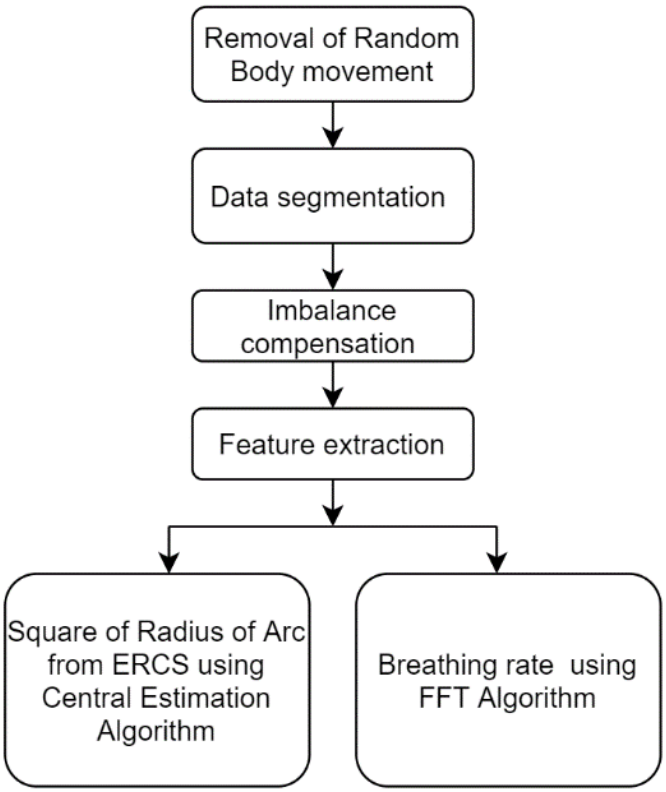

Fig 5.5: Flow chart for Feature Extraction Algorithm

Both KNN and SVM are supervised machine learning model that uses classification algorithms for two-group classification problems. After giving the model sets of labeled training data for each category, they're able to categorize new data. The same process is used here. Both breathing rate and square of radius of arc are used as features for normal, apnea and hypopnea events.

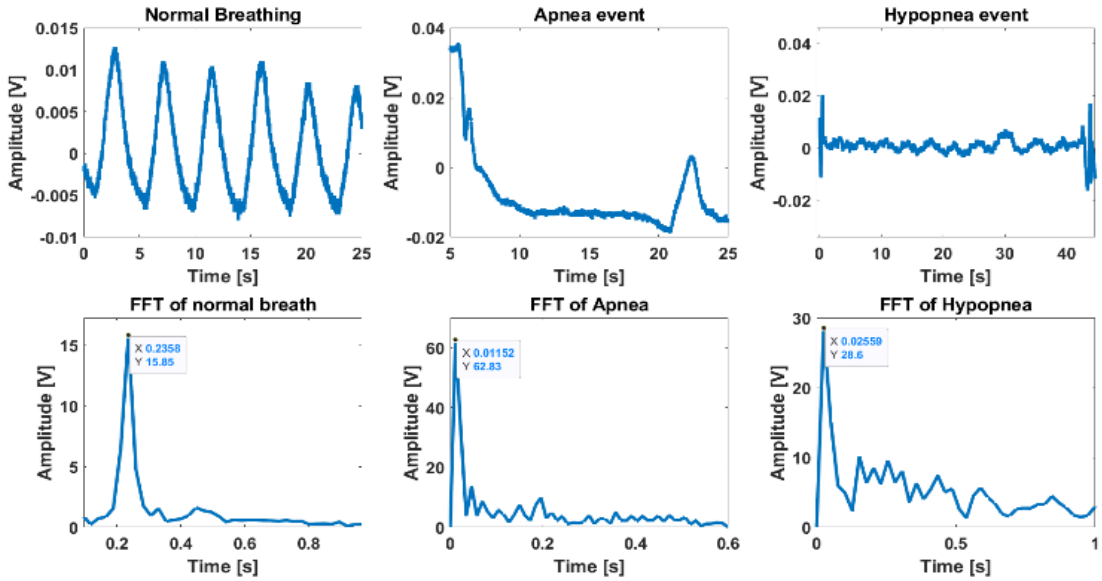

Fig 5.6: I/Q plot and corresponding Fast Fourier Transformation result of different OSA events (Normal, Hypopnea, and Apnea)

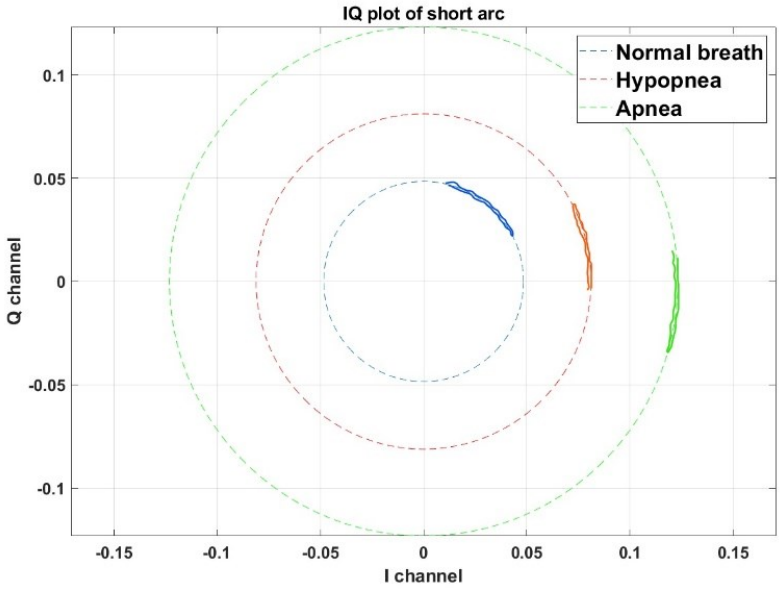

Fig 5.7: Central Estimation Algorithm tracked arc on circle drawn from different radius of arc, A for OSA patient in different OSA events (Normal, Hypopnea, Apnea), here square of Radius of Arc is directly proportional to ERCS

5.4 Result

Two different popular machine learning classifiers, K-nearest neighbor (KNN) and Support Vector Machine are integrated [99]. Two different kernel functions (Linear and Quadratic) are integrated which is used to mapping the non-linear function into linear mapping [99]. The data from all patients are analyzed in MATLAB (R2018b, The Math Works Inc., Natick, MA). To test performance of the integrated classifiers (KNN, SVM) a total set of 30 data set of each having 60 s epoch having three different patterns from five different participants. Table-I below shows the classification accuracy for different classifiers.

TABLE II
ACCURACIES FOR DIFFERENT CLASSIFIERS

Classifiers	**Training Accuracy**	**Test Accuracy**
KNN (1 Neighbor)	91%	89.2%
SVM (Linear)	96.67%	94.2%
SVM (Quadratic)	98.67%	96.7%

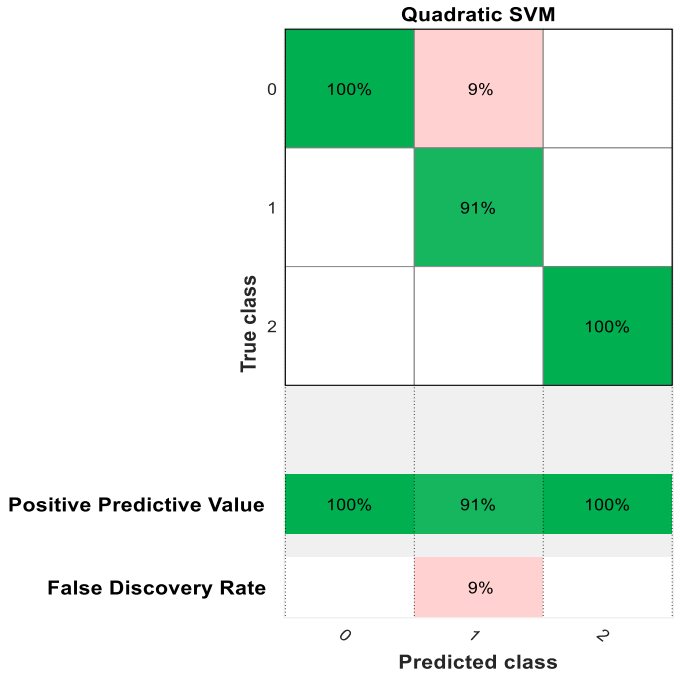

Fig 5.8: Confusion Matrix for Cubic SVM with respiration traces for ERCS and breathing rate measurement. (Class 0 represents normal breathing, class 1 apnea event and class 2 hypopnea event)

Testing data set is different than training data set, where 60% data set were used for training and 40% data set were used for testing. SVM with quadratic kernel function shows the best accuracy of 96.7% which outperformed other classifiers also. The confusion matrix of the testing data set is shown in Fig. 5.8.

The efficacy of ERCS methods to classify OSA events using Microwave Doppler radar which is integrated with machine learning classifier is tested. The experimental result demonstrated that, SVM with quadratic kernel outperformed KNN classifier with an accuracy of 96.7% to classify OSA events. As PSG system was used, the patients were sleeping in supine position. Since ERCS changes with sleep position, if sleep position changes, sleep apnea classification based on ERCS will be a more complex problem. Deep learning method will be investigated to solve this problem.

Chapter - 6

Orientation detection of Sedentary person

Sedentary means sitting for long periods. So, a person can do enough physical activity to meet the guidelines and still be considered sedentary if they spend a large amount of their day sitting or lying down at work, at home, for study, for travel or during their leisure time. It is a promising tool for medical monitoring, security applications, and smart buildings [100]. In some applications, such as in emergency search and rescue and occupancy sensing, orientation of a human subject with respect to the radar may not be known ahead of time. While human breathing and heartbeat can be measured from all four sides of the body [101], the characteristics of measured signals will vary with body orientation. Thus, it may not be possible to discern signal changes due to physiological response without information on body orientation with respect to the radar.

6.1 Experimental Setup

Human subjects represent a sophisticated target. Therefore, the experiment setup was designed with care to ensure precision of the alignment and accuracy of the readings. The CW Doppler radar motion sensor operation is based on capturing phase changes in the backscattered wave off the subject's torso that is phase modulated by the torso movement.

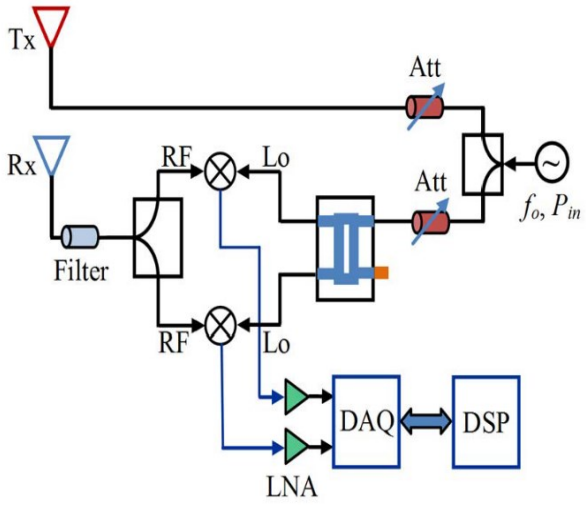

Fig 6.1: Schematic diagram of the CW Doppler system deployed for human testing [102]

A 2.4-GHz quadrature Doppler radar system was used for the experiment. The measuring system included a signal generator and the following off-the-shelf coaxial components: transmit and receive antenna (Antenna Specialist ASPPT2988), two 0° power splitters (Mini Circuits ZFC-2-2500), one 90° power splitter (Mini Circuits ZX10Q-2-25-S+), and two mixers (Mini- Circuits ZFM-4212). The retrieved signal from human subject is split and fed into two mixers. The local oscillator is connected to a quadrature power divider, providing in phase and quadrature version of the signal. The post processing is performed in MATLAB platform.

Fig 6.2: Setup for experiment inside an anechoic chamber. A subject sitting comfortably in front of doppler radar facing front at 1.1 m distance from radar

A healthy male subject was seated comfortably at 1.1 m from the radar (Fig. 2) on a chair without back support. The experiment procedures involving human subjects described in this paper were approved by the University of Hawaii Institutional Review Board, under protocol number CHS 14884. The radiating plane of transmitting and receiving antenna was perpendicular to the floor plane. The subject was measured while seated for three minutes in three different orientations (front, back, side) relative to Doppler radar. In each measurement scenario, the quadrature baseband signals were dc-coupled to the LNA's and dc cancelation was used. A system calibration procedure using spherical target was used to quantify and compensate amplitude and phase imbalance for IQ channels.

6.2 Parameter Variation of Sedentary person

When a human subject is the target, the parameters like motion rate, displacement magnitude and radar cross-section correspond to the respiration and heart rates, the torso motion depth, and the physical properties of the moving surface, respectively. Measurements of a subject in different sedentary positions aim to study the variation of these parameters with the angular orientation of the body and detect the effects of various positions.

6.2.1 Orientation

For the subject at fixed 1.1m target range, the measurements are taken at three different sedentary positions: front, back and side compared to radar. In front-faced, the subject sits comfortably on his/her back such that the Doppler radar monitors the front of the body. The arms are kept comfortably on the leg as shown in Fig. 6.3. In back, the subject seats on his/her front but unlike the chair in fig 6.3 it is actually a stool without any back. This way the chair do not interfere with the measurement and. In side position, the subject sits on his/her left side with the right side facing the antennas. The arms are kept away in the same position as shown in fig 6.3. The subject is asked to maintain a still position during the measurement and to breathe normally.

Fig 6.3: Different orientation of subject with respect to radar (side, back and front faced)

6.2.2 Respiration rate & Displacement

In the first set of measurements, the antennas are put at 1.1 m away and the 2.4 GHz system is ON. With the subject is seating front-faced to the radar, received signals are recorded while the subject is breathing for 90 seconds. Then the subject changes his position such that he seats with the back facing the transceiver antennas. The antennas position is kept the same and again, signals are recorded while subject breathing for 90 seconds. The same procedure is applied a third time for side position. In all measurements, the quadrature baseband signals are dc-coupled to the LNA's with closed-loop dc cancelation.

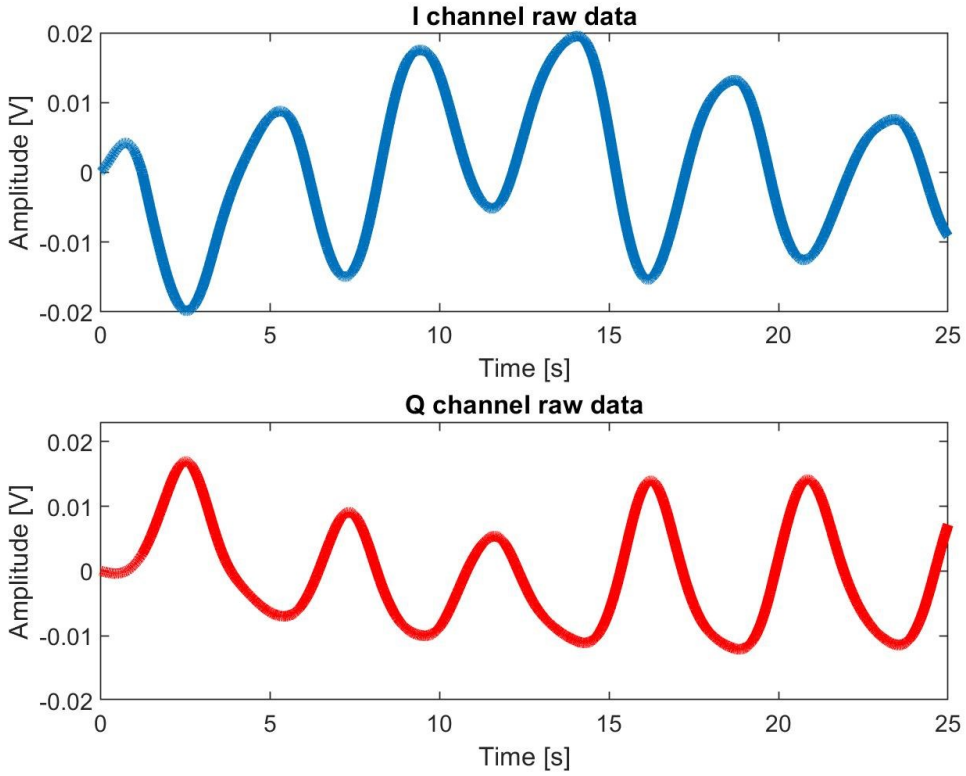

Fig 6.4: In-phase and quadrature raw data for subject front-faced at 1.1-m range.

The in-phase and quadrature signals are recorded separately but analyzed in pairs using the center estimation algorithm. The recorded raw data with the subject lying in supine are shown in Fig. 6.4. the Fourier analysis of the I-Q data with the subject in front-faced seating shows a peak at 0.233 Hz. The center estimation algorithm is applied to each data segment and the corresponding arc radius A is obtained. The result is a vector of length equal to the number of segments. A similar vector is obtained by applying the circle fitting algorithm to each segment of

data. The respiration rate is obtained from the data segmentation using the zero-crossing algorithm. Each segment corresponds to a full respiration cycle and is defined by three zero-crossings. The average segments length corresponds to the average respiration rate such that:

$$RR = 60xfs/\overline{Seg} \tag{6.1}$$

where RR is the average respiration rate in rpm, fs is the sampling frequency in Hz and Seg is the average number of samples per segment. The calculated average respiration rates are 12 rpm in front-faced, 13.9 rpm in back, and 11.2 rpm in side position.

The angle scanned by the arc on the complex I-Q plot corresponds to the displacement magnitude of the moving target. By measuring the scanned angle $\Delta\Omega$, the displacement is calculated using $\Delta x = \lambda \cdot \Delta\Omega / 4\pi$. With the change of orientation some major differences can be noticed. Along with change in respiration rate, displacement of the body surface also changes.

6.2.3 Radius of Arc

The in-phase and quadrature signals are two separately recorded but analyzed in pairs using the center estimation algorithm. The center-tracked arc for the subject in a front position is shown in Fig. 6.5. Only the arc corresponding to one segment of data is displayed. The arc lies on a circle centered at the origin of the coordinates as expected from the center estimation algorithm. When the subject switched to a back position, the dc-coupled arc is captured and center-tracked.

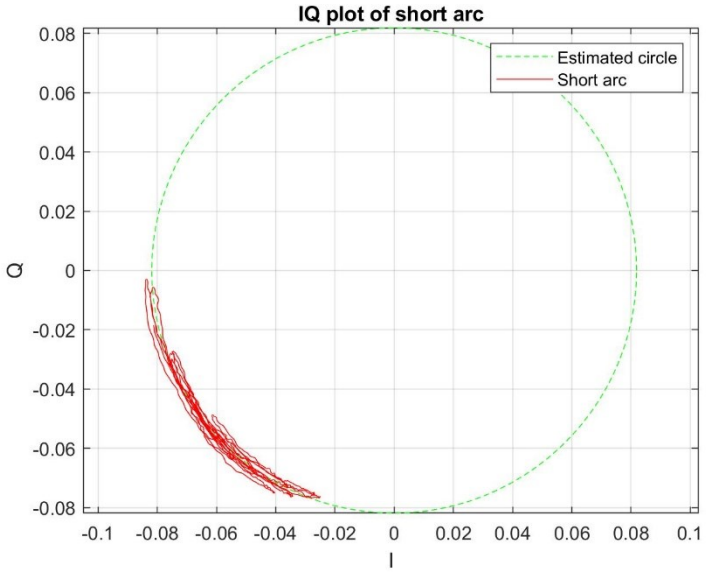

Fig 6.5: Radius of arc from I-Q data using center estimation algorithm in front sitting orientation

In general, the complex baseband signal may undergo some degradation due to noise or unintentional movement of the subject. The arc may also be too short and with a small curvature if the displacement of the body surface is too small during respiration. One of the major differences can be observed during the cardiopulmonary characteristics in different orientations of sedentary subject is radius of arc. The arc obtained from the body in the front position scans an angle $\Delta\Omega$ larger than that of the arc obtained from the back position. This is mainly due to the difference in the nature of motion at the body surface in the two orientations. When the subject sits front oriented compared to radar, he is breathing almost freely and all the motion of the respiration is translated to the front. When the subject sits back oriented compared to the radar, the motion of the thorax and abdomen are translated to a uniform motion of the back.

6.3 ERCS Variation due to geometry

The radar cross section measured for any moving target depends on the characteristics of its surface, namely size, curvature, and reflectivity. Since the surface moving during respiration is expected to be larger for larger subjects, the corresponding ERCS is expected to have a trend to vary with the physical dimensions of the subject's body. One essential dimension that affects the size of the moving surface during respiration is the chest breadth. This in turn affects the effective radar cross section measurement when the body is facing the incident wave in both the front and back-faced orientations.

The equation to calculate effective radar cross section, σ from all radar measurement parameter is:

$$\sigma = \frac{R^4}{Pin} \times \frac{1}{\Re} \times \left(\frac{A}{G}\right)^2 \tag{6.2}$$

where $\Re$ includes total fixed loss in the system, G is low noise amplifier gain, P_{in} is input power, R is range of the radar. The radius of the circle is A, and the angle scanned by the arc corresponds to the time-varying phase in the argument of both the cosine and sine. The radius A is estimated using the center estimation algorithm implemented in three steps [102]. From (6.2) it is evident that ERCS is directly proportional to square of radius of arc. For the subject, the calculated arc radius in back, front and side sitting positions with respect to the radar are 3V, 0.8V and 0.2V, respectively. it is evident that ERCS is largest for the back orientation, and smallest for the side orientation.

In general, the complex motion of human torso can be described by modeling the torso as a set of geometrical bodies that generally move with a spatially distributed phase. In Fig. 6.6, the front thorax and abdomen are represented by two separate cylindrical shells. The side body consists of another two shells that are vertically aligned with those of the front but with smaller radius of curvature. The back is mostly flat and is modeled as a rectangular sheet where the height equals to that of the torso and the width equals to the chest breadth [75]. In general, the size of the moving surface of the body that is exposed to incident wave is similar in the front and back positions. For the side position, the size of the exposed surface is reduced.

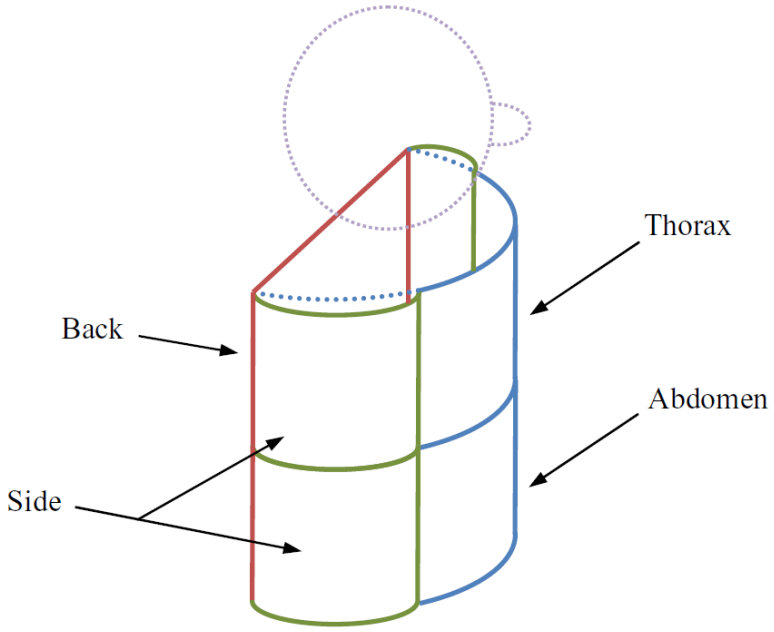

Fig 6.6: Geometrical model of human torso [75]

Since the surface moving during respiration is expected to be larger for larger subjects, the corresponding ERCS is expected to have a trend to vary with the physical dimensions of the subject's body. For a certain subject, due to the shape difference of the back of the body with respect to the front, the ERCS in a back orientation is expected to be different than that in front. This increase in radar cross section is due to the difference in geometrical shapes of the front and back of the body. The front of the body can be modeled as a cylinder with a radius of curvature roughly equal to half the chest breadth. As for the back of the body, the surface is flat enough to be modeled as a sheet with an area roughly equal to the chest breadth squared. According to literature [88], the radar cross section of a flat conducting sheet is larger than that of a cylinder of the same physical cross section area, especially in the optical region.

6.4 Result

The sampling frequency of the data acquisition (DAQ) was 100 Hz. Baseband signals were filtered using FIR filter of the order of 1000. FFT was used on arctangent demodulated signal to find the breathing rates. Fig. 6.7 illustrates the raw data, demodulated signal and the FFT of the demodulated signal. The center estimation algorithm is applied to each data segment and the corresponding arc radius is obtained.

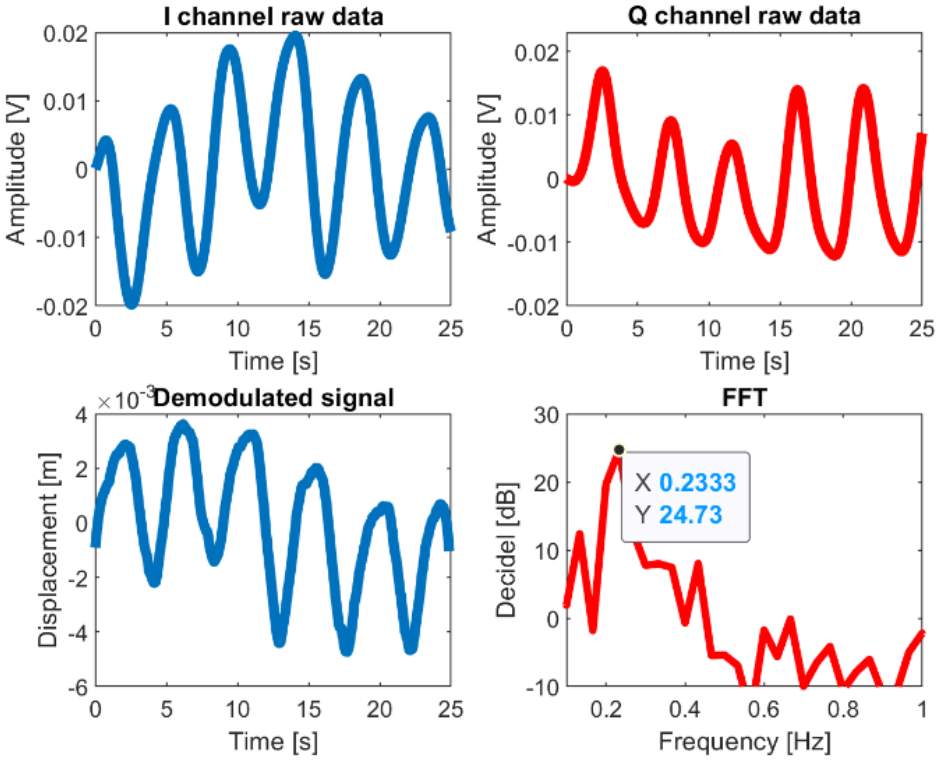

Fig 6.7: Radar captured raw data channel signal (a) In-phase (I) channel signal (b) quadrature phase (Q) signal (c) arctangent demodulated signal of chest displacement (d) FFT of the signal where peak of the signal illustrates the breathing rate of 0.23 Hz

Changing the position from front to back or side caused a variation in the detected ERCS of the body as well as the respiration characteristics in terms of respiration rate and respiration depth. For the subject, the calculated arc radius in back, front and side sitting positions with respect to the radar are 3V, 0.8V and 0.2V, respectively The difference in radius of arc for different sedentary orientation is represented in the fig 6.8.

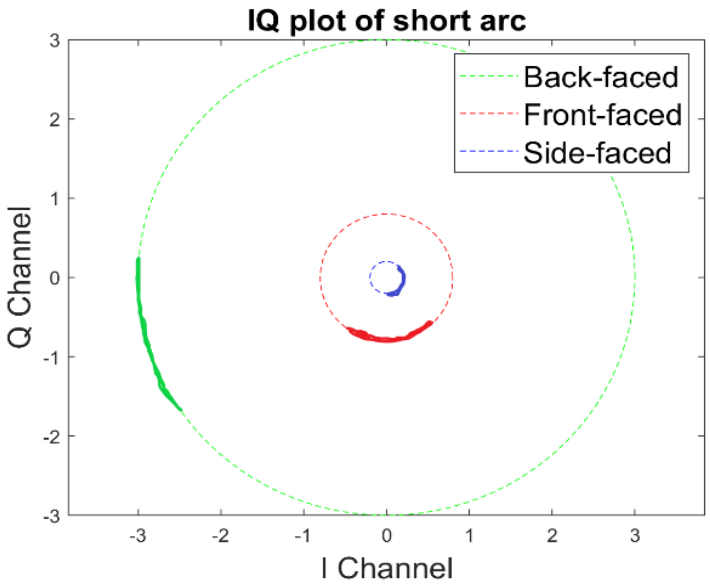

Fig 6.8: Center-tracked arcs for the subject in the front-faced, back-faced and side positions at 1.1-m range with 2.4 GHz carrier.

TABLE II
PARAMETER VARIATION OF DIFFERENT ORIENTATIONS FOR SEDENTARY PERSON

Orientation	Radius of Arc	Displacement	Respiration rate
Front	0.8V	0.75 cm	12 rpm
Back	3V	0.35 cm	13.9 rpm
Side	0.2V	0.22 cm	11.2 rpm

The analyses of data obtained from above table showed that the respiration depth of the subject is altered when the subject's position changed from front to back position. For instance, at 2.4 GHz carrier the measured displacement in back is 0.35 cm compared to 0.75 cm in front. This implies that the respiration depth is reduced approximately by a factor of 2 just by having the subject sitting in back instead of front. Similarly, in the side position the measured displacement was 0.22 cm, which is also smaller compared to that in front, this time by a factor of 3.4.The respiration depth reduction in back is expected as compared to front. But for the side position, while one side of the body is facing the hard surface, the other side is moving with a displacement proportional to the chest breadth span.

Chapter - 7

Summary

Doppler radar physiological monitoring provides a promising tool for monitoring heart and respiration signals without contact and through clothing. This technology can have numerous applications, such as sleep monitoring, home healthcare, baby monitoring, burn-injury victims, post-surgery monitoring, unique identification, search and rescue applications, see through the wall, gait characterization, indoor positioning, and occupancy detection. Although the technology has been around for a few decades, most of the advancements have been achieved during the past 10 years.

In general Radar cross-section is a measure of how detectable an object is by radar. Therefore, it is called electromagnetic signature of the object. A larger RCS indicates that an object is more easily detected. Its correlated with the geometry, reflectivity, material, and angle. In this thesis, Cardiopulmonary effective radar cross-section (ERCS) is discussed which is a measure of RCS due to moving part of human torso for respiration and heartbeat. Throughout the thesis, the definition, measurement process and hardware are discussed. Later part, the implementation, process, result of ERCS to classify obstructive sleep apnea (OSA) events and to identify orientation of sedentary subject has been discussed.

7.1 System Calibration:

The basic of continuous wave (CW) Doppler radar is explained in chapter 3. For the measurement of human cardiopulmonary ERCS using doppler radar has two aspects. One is RF system of doppler radar which defined the hardware part and next signal processing algorithm part. In the hardware part, the receiver, transmitter, channel type and the frequency are well defined as part of doppler radar architecture. The digital part means the algorithms for demodulate the signal and do further analysis to get physiological results.

After the design, it is necessary to quantify the system accuracy as well as the conditions at which the system works. RCS of a moving target is proportional to the power of the electromagnetic wave backscattered off the target. The reflected wave detected at the receiver is demodulated to obtain the baseband signal in form of two components in quadrature. On the complex I-Q plot, these components form an arc such that the radius of the arc is proportional to the square root of the radar cross section. The proportionality constant depends on the losses and gains encountered by the wave as it travels to the target and back to the receiver. The losses inherent to the system can be grouped into one factor that represents the total fixed gain in the system. This factor is independent of the system variables such as the target range and the

voltage gain of the LNA's. The round-trip gain factor can be directly measured if the RCS of the target used is already known. The units of this factor are in Wcm2. In the system calibration experiment, one target is used, a small metallic sphere having a 15.2-cm diameter. The target range satisfied the radiation far-field condition at 2.4 GHz.

7.2 Automated ERCS based classification of OSA events

The ability of Doppler radar to measure motion-based physiological parameters makes it suitable for the design of a non-contact sleep monitoring system. At present, the gold standard monitoring system is Polysomnography (PSG) which needs lots of contact sensors, expensive, hospital-based and obstructs natural sleep pattern of patients. Prior research has demonstrated the feasibility of utilizing Doppler radar-based system named physiological radar monitoring system (PRMS) to identify different apnea events in comparison to PSG system. The detailed parameter and system architecture of PRMS is discussed is section 3.8. But PRMS system was not automated. The system utilizes the amplitude-based technique to find different apnea events which requires extensive analysis and time-consuming.

In the thesis, machine learning algorithms has been used to classify OSA events. Supervised algorithm named KNN and SVM are used here, a brief description of these algorithms has been included in chapter 2. In chapter 5, I have investigated the feasibility of ERCS method for recognizing different OSA events (normal, apnea and hypopnea) from the clinical study with five different participants utilizing microwave Doppler radar system. The characterization of different OSA events based on breathing rate and ERCS which is proportional to square of radius of arc is explained. In addition to that, I have also integrated two different machine learning classifiers (KNN, SVM) to recognize different OSA events from ERCS and breathing rate measurement of the participants from different episodes of the clinical study. SVM with quadratic kernel outperformed other classifier with an accuracy of 96.7%. The proposed system has several potential applications especially in in-home sleep monitoring system for adults and infants also (Sudden Infant Death Syndrome).

7.3 ERCS based Orientation detection of Sedentary person

Prior research has been done on recognition of sleep position (supine, prone, normal) for recumbent subject using ERCS by John E. Kiriazi. The research proved that the ability to discriminate between the properties for different orientations is a key to monitor the position of the subject by remote sensing using Doppler radar. By analyzing the baseband signal into its quadrature components, digital processing algorithms can be applied to extract information about the subject's cardiopulmonary activity.

In smart building systems, Doppler radar may be used to help control heating, ventilation, air conditioning (HVAC), and lighting, to help optimize energy use. For such applications it is expected that human subjects will be mostly sedentary, and body orientation with respect to radar is not known ahead of time. Research has also been done also on measurement of physiological motions from four different body orientations for sedentary subject and orientation of recumbent subject. However, no prior work has been done to investigate the effect of different body orientations on ERCS for sedentary subjects. In this thesis, I have also investigated the ERCS changes due to different body orientations for sedentary subject. For this thesis, a subject was measured while seated for three minutes in three different orientations (front, back, side) relative to Doppler radar. In each measurement scenario, the quadrature baseband signals were dc-coupled to the LNA's and dc cancelation was used. For the subject, the calculated arc radius in back, front and side sitting positions with respect to the radar are 3V, 0.8V and 0.2V, respectively. ERCS in back position is the largest due to difference in geometrical shapes of the front, back and side of the body. This result agrees with previous work on ERCS for recumbent subject where ERCS for lying face-down is larger than face-up. These findings significantly extend the function of human Doppler radar cardiopulmonary monitoring, to provide robust comprehensive physiological monitoring capabilities for unattended subjects.

7.4 Challenge

One of the biggest challenges is measurement of ERCS correctly. Improper alignment of antenna will result in a reduction in the received power level and hence, in effective radar cross section. Correct alignment is important, any change in aspect angle will cause actual value reduction. RCS is dependent on parameter of the environment, so each time the environment changes, the system needs to be calibrated. The calibration of the system is also sensitive to alignment and frequency. The target needs to follow the far-field condition in indoor environment to get accurate ERCS value.

Unlike, RCS value ERCS is based on cardiopulmonary movement on human so its also dependent on the depth of breadth and the physical characteristics of the subject. That is why each time before taking the reading subject were given enough time to stabilize their respiration and heart rate. For multi-subject case all scenarios like physical characteristics effect, alignment effect and environmental effect need to be considered before coming to an conclusion. ERCS can give a lot of insight into how people orient and monitoring without being recorded by camera or contactless. But, the measurement technique is sensitive to some parameters which is need to be considered carefully before taking measurement.

7.5 Future work

A potential future work can focus on detecting the target misalignment and correct for it. The design of the system will need a direction of arrival detection that is possible with beam steering arrays. A detailed analysis on how change of depth of breadth affect RCS needs to be done. The calibration of the system mirroring the different breathing pattern with a known target can be a good future work.

The subject's physique acts an important role in measurement of RCS. This can be more explored on how the body structure affect tidal volume, respiration by looking more into ERCS variation. A detailed analysis with a number of subjects with different physical characteristics can help to come a proper conclusion. The orientation detection of sedentary measurement can be done for different people with different breathing pattern and how ERCS changes with that can be explored further.

For sleep monitoring system PSG system was used, the patients were sleeping in supine position. Since ERCS changes with sleep position, if sleep position changes, sleep apnea classification based on ERCS will be a more complex problem. In the thesis supervised machine learning algorithms have been implemented to classify OSA events. Deep learning method can be in the future investigated to solve this problem.

References

[1] Shahrokh Javaheri et al, “Sleep Apnea Types, Mechanisms, and Clinical Cardiovascular Consequences,” Journal of the American College of Cardiology, vol. 69, pp. 841-858, February 2017

[2] American College of Cardiology. https://www.acc.org/ Accessed 10th March, 2020

[3] Shekh M M Islam, Ashikur Rahman, Ehsan Yavari, Meheran Baboli, Olga Boric-Lubecke and Victor Lubecke, “Identity Authentication of OSA Patients Using Microwave Doppler Radar and Machine Learning Classifier”,*IEEE Radio Wireless Week(RWW’20),26-29 January, San Antonio, Texas,USA*

[4] M. Baboli, A. Singh, B. Soll, O. Boric-Lubecke and V. M. Lubecke, "Wireless Sleep Apnea Detection Using Continuous Wave Quadrature Doppler Radar," *IEEE Sensors Journal*, vol. 20, no. 1, pp. 538-545, 1 Jan.1, 2020

[5] J. E. Kiriazi, O. Boric-Lubecke and V. M. Lubecke, "Radar cross section of human cardiopulmonary activity for recumbent subject," *2009 Annual International Conference of the IEEE Engineering in Medicine and Biology Societ*y, Minneapolis, MN, 2009, pp. 4808-4811

[6] Rosalind Dymond Cartwright, “Effect of Sleep Position on Sleep Apnea Severity,” *Sleep,* vol no. 7, no. 2, pp. 110-114, September 1984

[7] A. Singh, M. Baboli, G. Xiaomeng, E. Yavari, B. Padasdao, B. Soll, et al., "Considerations for integration of a physiological radar monitoring system with gold standard clinical sleep monitoring systems," in Engineering in Medicine and Biology Society (EMBC), 2013 35th Annual International Conference of the IEEE, 2013, pp. 2120-2123

[8] ‘Sleep disorder.’ *Wikipedia https://en.wikipedia.org/wiki/Sleep_disorder* Accessed December 2019

[9] J.C. Lin, “Microwave sensing of physiological movement and volume change: A review,” *Bioelectromagnetics*, vol 13, no. 6, pp. 557-565, 1992

[10] M. I. Skolnik, "Radar," Encyclopedia Britannica

[11] J.C. Lin, “Microwave Propagation in Biological Dielectrics with Application to Cardiopulmonary Interrogation,” in *Medical Applications of Microwave Imaging, L.E. Larsen and J.H. Jacobi Ed., New York IEEE Press* pp. 47-58, 1986

[12] Y.F. Chen, D. Misra, H. Wang, H.-R.Chuang and E. Postow, “An X-Band Microwave Life-Detection System,” *IEEE Trans. Biomed*. Eng., vol. BME-33, no. 7, pp. 697-701, July 1986

[13] W. Massagram, V.M. Lubecke, A. Host-Madsen and O. Boric-Lubecke, “Assessment of Heart Rate Variability and Respiratory Sinus Arrhythmia via Doppler Radar,” *IEEE Trans. Microw. Theory Techn*., vol. 57, no. 10, pp. 2542-2549, Oct 2009

[14] J.Y. Lee, J.C. Lin, “A Microcprocessor-Based Noninvasive Arterial Pulse Wave Analyzer,” *IEEE Trans. Biomed. Eng*., vol. BME-32, no. 6, pp. 451-455, June 1985.

[15] Y.E. Moskalenko, “On the Application of Centimeter Radio Waves for Electrodeless recordings of volume changes of biological objects,” *Biophysics (USSR*), vol. 5, pp. 225-228, 1960.

[16] ‘Polysomnography’ *Wikipedia* https://en.wikipedia.org/wiki/Polysomnography Accessed December 2019

[17] L. Almazaydeh, "An interactive, real-time, high precision and portable monitoring system of obstructive sleep apnea," 3571495 Ph.D., University of Bridgeport, Ann Arbor, 2013.

[18] P. De Chazal, T. Penzel, and C. Heneghan, "Automated detection of obstructive sleep apnoea at different time scales using the electrocardiogram," *Physiol Meas*, vol. 25, pp.967-83, Aug 2004.

[19] P. De Chazal, C. Heneghan, and W. T. Mcnicholas, "Multimodal detection of sleep apnoea using electrocardiogram and oximetry signals," *Philos Trans A Math Phys Eng Sci*, vol. 367, pp. 369-89, Jan 28 2009

[20] A. Yilmaz and T. Dundar, "Home recording for pre-phase sleep apnea diagnosis by Holter recorder using MMC memory," in *Virtual Environments Human-Computer Interfaces and Measurement Systems* (VECIMS), 2010 *IEEE International Conference* on, 2010, pp. 126-129

[21] L. Derong, P. Zhongyu, and S. R. Lloyd, "A Neural Network Method for Detection of Obstructive Sleep Apnea and Narcolepsy Based on Pupil Size and EEG," *Neural Networks, IEEE Transactions on*, vol. 19, pp. 308-318, 2008

[22] T. Sugi, F. Kawana, and M. Nakamura, "Automatic EEG arousal detection for sleep apnea syndrome," *Biomedical Signal Processing and Control*, vol. 4, pp. 329-337, 2009.

[23] Yadollahi A, Moussavi Z., “Acoustic obstructive sleep apnea detection.” *Conf Proc IEEE Eng Med Biol Soc.* 2009

[24] Gehring J, Gesche H, Drewniok G, et al. “Nocturnal blood pressure fluctuations measured by using pulse transit time in patients with severe obstructive sleep apnea syndrome.” *Sleep Breath*. 2017

[25] Ishida R, Yonezawa Y, Maki H, et al. “A wearable, mobile phone-based respiration monitoring system for sleep apnea syndrome detection.” *Biomedical Sciences Instrumentation*. Vol. 41, pp. 289-293, 2005

[26] Rajalakshmi Nandakumar, Shyam Gollakota, Nathaniel Watson, “Contactless Sleep Apnea Detection on Smartphones”, *13th Annual International Conference on Mobile Systems, Applications and Services, 2015*

[27] K. Zhu et al, "Vision-Based Heart and Respiratory Rate Monitoring During Sleep – A Validation Study for the Population at Risk of Sleep Apnea," *IEEE Journal of Translational Engineering in Health and Medicine,* vol. 7, pp. 1-8, 2019, Art no. 1900708

[28] M. Baboli, "A Physiological radar system for diagnosing sleep disorders," 3648519 Ph.D., University of Hawaii, Manoa, 2014.

[29] Friedman, Jerome H. "Data Mining and Statistics: What's the connection?". *Computing Science and Statistics*. Vol. 29 (1), pp. 3–9, 1998

[30] “Machine Learning: An Introduction”, *towards datascience*, https://towardsdatascience.com/machine-learning-an-introduction Accessed July 2019

[31] “What is Machine Learning? A definition”, *Expert system* https://expertsystem.com/machine-learning-definition/ Accessed May 2020

[32] Garcia, Megan "Racist in the Machine". *World Policy Journal*, vol. 33 (4), pp. 111–117, 2016

[33] “K-Nearest Neighbors (KNN) Algorithm for Machine Learning”, *Medium,* https://medium.com/capital-one-tech/k-nearest-neighbors-knn-algorithm-for-machine-learning Accessed June 2019

[34] S. V. M. Vishwanathan and M. Narasimha Murty, "SSVM: a simple SVM algorithm," *International Joint Conference on Neural Networks*., vol.3, pp. 2393-2398, 2002

[35] J. Muehlsteff, J. Thijs, R. Pinter, G. Morren, and G. Muesch, "A handheld device for simultaneous detection of electrical and mechanical cardio-vascular activities with synchronized ECG and CW-Doppler Radar," in *Engineering in Medicine and Biology Society*, 2007. EMBS 2007. 29th Annual *International Conference of the IEEE*, 2007, pp. 5758-5761

[36] K. Mostov, E. Liptsen, and R. Boutchko, "Medical applications of shortwave FM radar: Remote monitoring of cardiac and respiratory motion," *Medical Physics*, vol. 37, pp. 1332-1338, 2010

[37] D. Qiao, T. He, B. Hu, and Y. Li, "Non-contact physiological signal detection using continuous wave Doppler radar," *Bio-Medical Materials and Engineering*, vol. 24, pp. 993-1000, 01/01/ 2014.

[38] A. Droitcour, V. Lubecke, L. Jenshan, and O. Boric-Lubecke, "A microwave radio for Doppler radar sensing of vital signs," in *Microwave Symposium Digest*, 2001 IEEE MTTS International, 2001, pp. 175-178 vol.1.

[39] A. D. Droitcour, O. Boric-Lubecke, V. M. Lubecke, and L. Jenshan, "0.25 /spl mu/m CMOS and BiCMOS single-chip direct-conversion Doppler radars for remote sensing of vital signs," in *Solid-State Circuits Conference*, 2002. *Digest of Technical Papers*. ISSCC. 2002 *IEEE International*, 2002, pp. 348-349 vol.1

[40] A. D. Droitcour, O. Boric-Lubecke, V. M. Lubecke, J. Lin, and G. T. A. Kovacs, "Range correlation effect on ISM band I/Q CMOS radar for non-contact vital signs sensing," in *Microwave Symposium Digest*, 2003 *IEEE MTT-S International*, 2003, pp. 1945-1948 vol.3.

[41] M. I. Skolnik, *Introduction to radar systems*: McGraw-Hill, 1962

[42] W. Massagram, A Study of Feasibility in Long-term Cardiopulmonary Monitoring Via Doppler Radar: University of Hawai'i at Manoa, 2008.

[43] M. I. Skolnik, *Introduction to Radar Systems*: Tata McGraw Hill, 2003

[44] S. Kingsley and S. Quegan, Understanding Radar Systems: Institution of Engineering and Technology, 1999.

[45] E. Aries, M.F. MacDorman, D. M. Strobino and B. Guyer, "Annual summary of vital statistics – 2002," *Pediatrics*, vol. 112, no. 6, pp. 1215-1230, 2003

[46] S. M. Domer, S. A. Foertsch, and G. D. Raskin, "Model for yield and manufacturing prediction on VLSI designs for advanced technologies, mixed circuitry, and memories," *IEEE Journal of Solid-State Circuits*, vol. 30, no. 3, pp. 286 - 294, 1995.

[47] K. H. Chan and J. C. Lin, "Microprocessor-based cardiopulmonary rate monitor," *Medical and Biological Engineering and Computing*, vol. 25, no. 9, pp. 41-44, 1987.

[48] K.-M. Chen, Y. Huang, J. Zhang, and A. Norman, "Microwave life-detection systems for searching human subjects under earthquake rubble or behind

barrier," *IEEE Transactions of Biomedical Engineering*, vol. 47, no. 1, pp.105-114, 2000

[49] H.-R. Chuang, Y.-F. Chen, and K.-M. Chen, "Microprocessor-controlled automatic clutter-cancellation circuits for microwave systems to sense physiological movements remotely through the rubble," *Instrumentation and Measurement Technology Conference*, 1990, pp. 177-181.

[50] J. Seals, S. R. Crowgey, S.M. Sharpe, "Electromagnetic vital signs monitor" Georgia Tech Research Institute Biomedical Division, Atlanta, GA, Final Report Project A-3529-060, 1986.

[51] T. Matsui, T. Ishizuka, B. Takase, M. Ishihara, and M. Kikuchi, "Non-contact determination of vital sign alterations in hypovolemic states induced by massive hemorrhage: an experimental attempt to monitor the condition of injured persons behind barriers or under disaster rubble," *Medical and Biological Engineering and Computing*, vol. 42, no. 6, pp. 807-811, 2004.

[52] T. Matsui, K. Hagisawa, T. Ishizuka, B. Takase, M. Ishihara, and M. Kikuchi, "A novel method to prevent secondary exposure of medical and rescue personnel to toxic materials under biochemical hazard conditions using microwave radar and infrared thermography," *IEEE Transactions on Biomedical Engineering*, vol. 51, no. 12, pp. 2184-2188, 2004.

[53] O. Boric-Lubecke, G. Atwater, and V. M. Lubecke, "Wireless LAN PC card sensing of vital signs," *IEEE Topical Conference on Wireless Communications Technology*, 2003, pp. 206-207.

[54] V. Lubecke, O. Boric-Lubecke, and E. Beck, "A compact low-cost add-on module for Doppler radar sensing of vital signs using a wireless communications terminal," *IEEE Microwave Theory and Techniques Symposium Digest*, 2002, pp. 1767-1770.

[55] O. Boric-Lubecke and V. M. Lubecke, "Wireless house calls: Using communications technology for health care monitoring," *IEEE Microwave Magazine*, vol. 3, no. 3, pp. 43-48, 2002

[56] I. Y. Immoreev and S. Samkov, "Short-distance ultrawideband radars," *IEEE Aerospace and Electronic Systems Magazine*, vol. 20, no. 6, pp. 9-14, 2005.

[57] G. Ossberger, T. Buchegger, E. Schimback, A. Stetzler, and R. Weigel, "Non-invasive respiratory movement detection and monitoring of hidden humans

using ultra-wideband pulse radar," *the International Workshop on Ultrawideband Technologies*, 2004, pp. 395-399

[58] D. Matsumoto and Y. Kuwahara, "Heartbeat and respiratory monitoring using standing wave radar and independent component analysis," in *International Symposium on Antennas and Propagation* (ISAP), 2016.

[59] V. M. Lubecke, *Continuous Non-Contact Sensor Technology for Sleep Monitoring*, Manoa, 2013.

[60] L. Ren, M. S. Hasan, S. K. Islam, A. E. Fathy and R. A. Fathy, "UWB baby and sleep apnea monitor," in *IEEE International Symposium on Antennas and Propagation & USNC/URSI National Radio Science Meeting*, San Diego, California, July 2015.

[61] A. D. Droitcour, "Non-contact measurement of heart and respiration rates with a single-chip microwave doppler," Ph.D., Stanford University, 2006.

[62] A. A. Abidi, "Direct-conversion radio transceivers for digital communications," *IEEE Journal of Solid State Circuits*, vol. 30, no. 12, pp. 1399-1410, 1995

[63] Graf, Rudolf F., "Modern dictionary of electronics" (7th ed.). USA: Newnes. p. 344, (1999).

[64] Horowitz, Paul; Hill, Winfield, "The Art of Electronics", (2nd ed.) London: Cambridge University Press. pp. 885, 897, 1989

[65] Hogan, John V. L., "The Heterodyne Receiver", *Electric Journal*, vol. 18, pp. 116, 1921

[66] Nahin, Paul J., "The Science of Radio with Matlab and Electronics Workbench Demonstrations" (2nd ed.), New York: Springer-Verlag, 2001

[67] I. Mostafanezhad, "Noise reduction techniques for wireless life signs devices," 3415883, Ph.D., University of Hawaii, Manoa, 2010.

[68] B.-K. Park, A. Vergara, O. Boric-Lubecke, and V. M. Lubecke, "Signal coupling effects on quadrature demodulation accuracy of Doppler radar motion detector," *IEEE Trans. on Biomedical Circuits and Systems*, September 2010.

[69] B.-K. Park, O Boric-Lubecke, and V. M. Lubecke, and A. Host-Madsen, "Optimum demodulation for Doppler radar heart sensing," *IEEE Signal Processing Letters*, 2010.

[70] F. Jay, (editor in chief*), IEEE Standard Dictionary of Electrical and Electronics Terms, ANSI/IEEE* Std 100-1984, 3rd edition, IEEE Press, New York, 1984

[71] A. Vergara and V. Lubecke, "Data acquisition system for Doppler radar vital-sign monitor," *Engineering in Medicine and Biology Society*, 2007. EMBS 2007. 29th *Annual International Conference of the IEEE*, pp. 2269–2272, Aug. 2007.

[72] C. Li and J. Lin, "Complex signal demodulation and random body movement cancellation techniques for non-contact vital sign detection," *Microwave Symposium*, 2008*, IEEE/MTT-S International*, pp. 567-570, June 2008.

[73] B.-K. Park, O. Boric-Lubecke, and V. M. Lubecke, "Arctangent demodulation with dc offset compensation in quadrature Doppler radar receiver systems," *Microwave Theory and Techniques, IEEE Transactions* on, vol. 55, no. 5, pp. 1073–1079, May 2007.

[74] A. Vergara, O. Boric-Lubecke, and V. M. Lubecke, "DC information preservation for cardiopulmonary monitor utilizing CW Doppler radar", 30th *Annu. Conf. IEEE EMBS*, Vancouver, BC, 2008, pp. 1246-1249.

[75] J. E. Kiriazi, "Human cardiopulmonary recognition using close-range doppler radar," 3448678, Ph.D., University of Hawaii, Manoa, 2010.

[76] B. Lohman, O. Boric-Lubecke, V. M. Lubecke, and P. W. Ong, M. M. Sondhi, "A digital signal processor for Doppler radar sensing of vital signs," *IEEE Engineering in Medicine and Biology Magazine*, vol. 21, pp. 161-164, Sept-Oct. 2002

[77] Embla. https://embla.com.au/ Accessed May 2019

[78] Clevemed. https://clevemed.com/ Accessed February 2019

[79] Queens Medical. http://queensmedicalcenter.org/ Accessed May 2018

[80] W. Xiaoyue, C. Mingqui, L. Macchiarulo, and O. Boric-Lubecke, "Fully-Integrated Heart Rate Variability Monitoring System with an Efficient Memory," in *Engineering in Medicine and Biology Society*, 2006. EMBS '06. 28th *Annual International Conference of the IEEE*, 2006, pp. 5064-5067.

[81] Mini Circuits. Coaxial Power Splitter/Combiner. Available: http://www.minicircuits.com/pdfs/ZFSC-2-2500.pdf [Accessed: July 20, 2014]

[82] Datasheet Archive. (2014). ASPPT2988 data sheet. Available: http://www.datasheetarchive.com/ASPPT2988-datasheet.html

[83] Mini Circuits. ZFM-4212 Coaxial Fequency Mixer. Available: http://www.minicircuits.com/pdfs/ZFM-4212+.pdf [Accessed: July 20, 2014]

[84] Stanford Research Systems. Preamplifier SR560. Available: http://www.thinksrs.com/products/SR560.htm

[85] Rf Beam Microwave Gmbh. (2014). K-MC1 Radar Transceiver. Available: http://www.rfbeam.ch/products/k-mc1-transceiver/ [Accessed: 2014]

[86] National Instruments. (2014). NI USB-6259 Screw Terminal. Available: http://sine.ni.com/nips/cds/view/p/lang/en/nid/202803 [Accessed: July 20, 2014]

[87] E. F. Knott, J. F. Shaeffer, and M. T. Tuley, *Radar Cross Section*, 2nd ed., Norwood, MA: Artech House, 1993.

[88] M. L. Skolnik, Introduction to Radar Systems, 3rd ed., New York: McGraw-Hill Inc., 2001.

[89] R. G. Kouyoumjian and L. Peters, Jr., “Range requirements in radar cross section measurements,” *IEEE*, vol. 53, August 1965, pp. 920-928.

[90] E. F. Knott and T. B. A. Senior, “How far is far?” *Antennas and Propagation, IEEE Transactions on*, vol. AP-22, pp. 732-734, September 1974.

[91] K. Konno and J. Mead, “Measurement of the separate volume changes of rib cage and abdomen during breathing,” *J Appl Physiol*, vol. 22, no. 3, pp. 407–422, 1967.

[92] I. Sato and M. Nakajima, “Non-contact Breath Motion Monitoring System in Full Automation,” 27th *Annu. Conf. IEEE EMBS*, Shanghai, 2005, pp. 3448-3451.

[93] L. Marcus and W. Peter, “Radar reflecting target for reducing radar cross section,” *International Patent* WO 90/13926, November 15, 1990.

[94] RB Dybdal, “Radar Cross Section Measurements,” *IEEE Proceedings*, vol. 75, no. 4, April 1986.

[95] M Zakrzewski, A Singh, E Yavari, X Gao, ” Quadrature imbalance compensation with ellipse-fitting methods for microwave radar physiological sensing,” *IEEE Transactions on Microwave Theory and Techniques,* vol 62(6), pp. 1000-1008, 2014

[96] Iber C, Ancoli-Israel S, J. Chesson Al, and Q. Sf, "The AASM manual for the scoring of sleep and associated events: rules, terminology and technical specifications," 1 ed. American Academy of Sleep Medicine, 2007

[97] Y. Castillo-Escario, I. Ferrer-Lluis, J. M. Montserrat and R. Jané, "Entropy Analysis of Acoustic Signals Recorded With a Smartphone for Detecting Apneas and Hypopneas: A Comparison With a Commercial System for Home Sleep Apnea Diagnosis," *IEEE Access*, vol. 7, pp. 128224-128241, 2019

[98] Scott L. DeBoer, “Emergency Newborn Care.” *Trafford Publishing*. p. 30, November 2004

[99] Corinna Cortes and Vladimir Vapnik, “Support Vector Networks,” *Machine Learning (Springer)*, vol. 20(3), pp. 273-297, September 1995

[100] Ehsan Yavari, Chenyan Song, Victor Lubecke and Olga Boric-Lubecke, “Is there anybody in there?: Intelligent radar occupancy sensors”, *IEEE Microwave Magazine*, vol. 15, no. 2, 2014, pp. 57-64.

[101] Changzhi Li, Victor M. Lubecke, Olga Boric-Lubecke, Jenshan Lin, “A Review on Recent Advances in Doppler Radar Sensors for Noncontact Healthcare Monitoring”, *IEEE Transactions on Microwave Theory and Techniques*, vol. 65, no. 5, 2017, pp. 1692-1706.

[102] John E. Kiriazi, Olga Boric-Lubecke, and Victor M. Lubecke, “Dual-Frequency Technique for Assessment of Cardiopulmonary Effective RCS and Displacement”, *IEEE Sensors Journal*, vol. 12, no. 3, 2012, pp. 574-582.